This article has been accepted for publication in a future issue of this journal, but has not been fully edited. Content may change prior to final publication.
Citation information: DOI: 10.1109/TSG.2025.3586757, IEEE Transactions on Smart Grid

Integrated Underfrequency Load Shedding Strategy for Islanded Microgrids Integrating Multiclass Load-related Factors

Can Wang, *Member*, *IEEE*, Bentao Cheng, Xuhui He, Lei Xi, Nan Yang, *Senior Member*, *IEEE*, Zhuoli Zhao, Chun Sing Lai, *Senior Member*, *IEEE*, and Loi Lei Lai, *Life Fellow*, *IEEE*

***Abstract*—Reducing the decision response time of load shedding while considering the comprehensive value of load shedding is one of the main challenges faced in emergency control of islanded microgrids. However, the existing underfrequency load shedding strategies do not fully consider the multiple factors associated with the load, and load assessment and load shedding decision-making are separated; this results in a long response time for underfrequency load shedding decisions for islanded microgrids. Therefore, in this paper, an integrated underfrequency load shedding strategy for islanded microgrids is proposed, which integrates multiclass load-related factors. This strategy first constructs an integrated underfrequency load shedding model for islanded microgrids on the basis of multiclass load-related factors such as the load frequency regulation effect, load shedding cost, and three-phase system power unbalance degree. Then, the load shedding model is described as a Markov decision process (MDP), and the environment, action space, and reward function are defined considering the load shedding objectives and constraints of islanded microgrids. Finally, a novel twin delay deep deterministic policy gradient method with softmax and dual buffer replay (DBR-SD3) is developed to determine the optimal integrated underfrequency load shedding strategy. This approach integrates softmax and the dual buffer replay mechanism into twin delay deep deterministic policy gradient (TD3), which greatly improves the ability of the agent to learn the optimal load shedding strategy in a complex microgrid operating environment. The simulation results based on the improved IEEE 37-bus microgrid and IEEE 118-bus microgrid verify that the proposed integrated load shedding strategy can greatly reduce the decision response time, correct the three-phase power unbalance of the system while minimizing the load shedding cost, and restore the system frequency to a normal level more quickly. Moreover, even under strong noise interference, the proposed strategy can produce stable load shedding decisions and has strong robustness and adaptability.**

***Index Terms*—microgrid, underfrequency load shedding, load-related factors, DBR-SD3.**

This work was supported by the National Natural Science Foundation of China under Grant 62233006. Paper no. TSG-01746-2024(*Corresponding author: Can Wang*)

Can Wang, Bentao Cheng, Lei Xi, and Nan Yang are with the College of Electrical Engineering and New Energy and Hubei Provincial Engineering Technology Research Center for Microgrid, China Three Gorges University, Yichang 443002, China (e-mail: xfcancan@163.com; 17362360267@163.com; xilei2014@163.com; ynyyayy@ctgu.edu.cn).

Xuhui He is with the State Grid Jingzhou Power Supply Company, Jingzhou 434000, China (email: xuhui_h@163.com).

Z. Zhao, and L. L. Lai are with the Department of Electrical Engineering, School of Automation, Guangdong University of Technology, Guangzhou, 510006, China (e-mail: zhuoli.zhao@gdut.edu.cn; l.l.lai@ieee.org).

C. S. Lai is with the Department of Electronic and Electrical Engineering, Brunel University London, London, UB8 3PH, UK (e-mail: chunsing.lai@brunel.ac.uk).

I. Introduction

With the gradual increase in smart grid construction in China, the penetration rate of distributed generators (DGs), which are powered primarily by new energy in microgrids, is increasing daily [1], [2]. However, DGs need to be connected to the power grid through power electronic equipment, and their frequency recovery ability is weak, which may cause problems such as frequency safety and stability issues when serious faults occur. Especially for islanded microgrids, postfault frequency instability is an important cause of economic losses [3]. When a fault occurs in an islanded microgrid, if effective emergency intervention measures cannot be taken in time, it may lead to chain failure or power outages in the whole network [4]. To minimize the adverse effects of fault events on islanded microgrids, the frequency recovery problem must be effectively addressed.

To enable the frequency of the islanded microgrid system to recover to a stable state after a disturbance quickly, a multi-stage droop control parameter optimization method was proposed in [5]. This method optimizes the power output strategy of DGs by adaptively modifying the droop control parameters to recover the frequency deviation caused by unexpected disturbances quickly. A distributed control strategy was designed in [6]. This strategy can control the energy storage system to participate in different frequency regulation tasks and effectively reduce the frequency variation caused by power fluctuations. To fully utilize the ability of each unit in the microgrid to regulate the system frequency, an adaptive control strategy that combines decentralized and distributed technologies was proposed in [7]. This strategy coordinates the output power amount of each unit according to the inverter capacity of photovoltaic and energy storage, thus maintaining the microgrid frequency in a safe and stable state. All of the above research has proposed different control strategies to optimize the frequency regulation capability of microgrids from the source-side perspective. However, when faced with an emergency scenario in which the power output has reached the upper limit but still cannot effectively suppress the frequency drop, the above control strategies cannot further play the role of frequency regulation. As an important means of emergency control of a power system, underfrequency load shedding can prevent a rapid drop in system frequency by cutting off part of the load when the power output is saturated ensure the safety of the system frequency [8], [9]. Therefore, it is crucial to design an effective and reasonable underfrequency load shedding (UFLS) strategy for the safe and stable operation of islanded microgrids.

As research on UFLS increases, the traditional load-shedding problem has been constructed as a variety of mathematical and

This article has been accepted for publication in a future issue of this journal, but has not been fully edited. Content may change prior to final publication.
Citation information: DOI: 10.1109/TSG.2025.3586757, IEEE Transactions on Smart Grid

physical models to find the optimal load shedding scheme [10-12]. In [10], an adaptive undervoltage load shedding scheme based on model predictive control (MPC) was proposed, which introduced the concept of voltage and reactive power variables to alleviate voltage instability in the case of unexpected faults. In [11], an adaptive load-shedding strategy based on a comprehensive evaluation of the frequency and voltage stability of synchronous phasor measurements was proposed. This strategy allocates load shedding according to the voltage and frequency information provided by the phasor measurement units (PMUs) to improve the stability of voltage and frequency recovery. In [12], a dynamic multistage underfrequency load shedding strategy considering generation loss uncertainty was proposed, which describes the UFLS problem as a mixed integer linear programming optimization problem to minimize load shedding. However, the above methods rely on the system model, require high-accuracy models, and have problems with poor scalability and long model solving times. When applied to emergency control of a power grid, the instantaneous response effect is poor.

In recent years, methods based on machine learning (ML) have shown great potential in the field of microgrid control [13], [14]. Unlike traditional modeling methods, methods based on ML can output control decisions in a short time. In [15], a two-stage load shedding strategy was proposed, which first uses a support vector machine to evaluate the stability of the system and then performs load shedding according to a predefined scheme. In [16-17], an extreme learning machine model was trained according to pregenerated load-shedding data, and then the trained model was used to predict the amount of load shedding. However, these traditional ML models rely on high-quality databases, and their data processing is more complex. In this context, a coordinated load shedding control strategy for islanded microgrids based on the Q learning framework was proposed in [18], which uses a Q value table to record the data values in the model training process, greatly reducing the workload of data processing. However, Q learning encounters dimensional disasters in high-dimensional spaces, which greatly limits the application of this strategy. To solve this problem, deep reinforcement learning (DRL), which organically integrates deep learning and reinforcement learning, has been widely researched and applied. A novel adaptive emergency control scheme was designed on the basis of the high-dimensional feature extraction and nonlinear generalization capabilities of the deep Q-network (DQN) in [19]. However, as a discrete control-oriented method, the DQN cannot output the optimal Q values for continuous actions. In [20], a frequency control method based on deep deterministic policy gradient (DDPG), which can address continuous states and actions, was proposed. In [21], an adaptive power tracking control method integrating adaptive learning and DDPG was proposed, which can adaptively adjust DDPG model parameters according to the control effect. To solve the problem of poor adaptability of traditional DRL in the face of new tasks, a frequency control method for islanded microgrids based on deep meta deterministic policy gradient was proposed in [22], which introduces meta-learning into DDPG to guide agents to perform multi-task collaborative learning through meta-learning, thereby enhancing the adaptability of the model in different fault scenarios. However, the DDPG is more sensitive to parameter settings, and overestimating the Q value leads to the failure of the learned strategy. A frequency regulation method based on TD3 was proposed in [23], which effectively reduces the problem of overestimation of the Q value. In [24], a load restoration strategy for a distribution network based on TD3 was proposed, which significantly improves the model's generalization ability to untrained scenarios by introducing meta-learning. However, the conservative value function estimation method of TD3 may lead to underestimation, causing the agent to only learn suboptimal strategies.

It is also notable that in the microgrid system, in addition to many three-phase loads, there are also some single-phase source–load–storage components, and these single-phase components will cause a three-phase unbalance in the system. The method of virtual three-phase combination sorting of heterogeneous sources, loads, and storage was proposed in [25-26] to effectively avoid the issue of three-phase system power unbalance in the passive parallel transfer process for the microgrid. However, the above studies first preprocess the load through virtual combination and evaluation to obtain the contribution value of the load and then construct a set of load shedding actions on the basis of this contribution value and execute the load shedding actions. This method of first evaluating and then reducing the load increases the response time of the system's load shedding actions, thereby impacting the frequency recovery of the system. In addition, the load-cutting method based on virtual combination has strong limitations and must be used in the initial island equilibrium state. For an islanded microgrid with unbalance at the initial time, the load-cutting method of virtual combination may increase the unbalance and the operating loss of the system.

Considering the shortcomings of the above research, this paper proposes an integrated underfrequency load shedding strategy for islanded microgrids that integrates multiclass load-related factors. The proposed strategy fully considers the influence of multiclass load-related factors on the system load shedding process and combines the two separate processes of load assessment and underfrequency load shedding into one to obtain a new integrated load shedding mode, which overcomes the defects of long response times caused by insufficient consideration of load factors and the independence of load assessment and load shedding decisions in current load shedding decision-making. In addition, the proposed strategy uses a new twin delayed deep deterministic policy gradient with softmax and dual buffer replay (DBR-SD3) method based on a continuous action space for learning load shedding decisions, effectively improving the learning efficiency and quality of decision-making. When a power shortage occurs in an islanded microgrid due to faults, the proposed strategy can effectively prevent rapid frequency drops in the system, ensuring the reliability of important load supply with lower load shedding costs while correcting three-phase power unbalance issues during system operation.

The main contributions of this paper are as follows:

(1) A three-phase unbalanced load shedding correction method suitable for multiple scenarios is proposed. Unlike in [25-26], the strategy proposed in this paper directly determines the optimal underfrequency load shedding strategy through DRL for agents. The application scenario of the proposed strategy is not limited by the initial three-phase unbalance degree of the system and can quickly restore the system frequency while correcting the unbalanced operations of the system. In the modified IEEE 37-bus and IEEE 118-bus systems, the proposed strategy 1 reduced the system power unbalance by 7.69% and 5.86%, respectively

This article has been accepted for publication in a future issue of this journal, but has not been fully edited. Content may change prior to final publication.
Citation information: DOI: 10.1109/TSG.2025.3586757, IEEE Transactions on Smart Grid

compared to before the load shedding operation, while the system the power unbalance of the system increased under the MPC-based load shedding strategy 2, DDPG-based load shedding strategy 3, and DQN-based load shedding strategy 4. The proposed strategy achieved the best unbalance improvement effect.

(2) An integrated underfrequency load shedding mode for islanded microgrids is proposed. Unlike the load shedding mode that load assessment and load shedding are separated from each other in references [7], [17] and [19], the proposed strategy uses the DRL method to combine load assessment and underfrequency load shedding into one process, which greatly reduces the response time of the load shedding decision. In addition, unlike in reference [7], the proposed strategy is less affected by the accuracy of physical or mathematical models and has strong scalability, so it can provide optimal load shedding control actions quickly and stably. In the modified IEEE 37-bus system, the online calculation time of the proposed strategy is 0.032 seconds, which reduces strategies 2, 3, and 4 by 58.44%, 23.81%, and 38.46%, respectively. In the modified IEEE 118-bus system, the online calculation time of the proposed strategy is 0.092 seconds, which is reduced by 45.24%, 9.8%, and 22.03% compared to strategies 2, 3, and 4, respectively. The strategies proposed in different bus systems have achieved the fastest online response speed.

(3) A new DRL method, DBR-SD3, is proposed for generating optimal load shedding strategies. Unlike traditional DRL methods, the proposed DBR-SD3 performs accurate estimation of the Q values during parameter training by integrating the softmax function with TD3. Moreover, to further improve the quality of the optimal strategy, a dual buffer replay mechanism is adopted to improve the learning speed and convergence stability of the strategy. Training performance analysis shows that the speed of the proposed DBR-SD3 to learn the optimal load shedding control strategy is about 1.5/3.25/3.5 times that of TD3/DDPG/DQN, respectively, and the average reward obtained during convergence is increased by 34.46%, 45.94%, 65.54% based on TD3/DDPG/DQN. The proposed strategy shows obvious advantages in convergence speed and convergence quality.

The rest of this paper is organized as follows: Section II describes an integrated underfrequency load shedding model for islanded microgrids. Section III converts the underfrequency load shedding problem for islanded microgrids into an MDP. Section IV provides a detailed introduction to the proposed strategy training and integrated load shedding strategy framework. Section V evaluates the performance of the proposed method through simulation analysis. Finally, section VI provides a summary of the entire paper.

II. INTEGRATED UNDERFREQUENCY LOAD SHEDDING MODEL FOR ISLANDED MICROGRIDS

The load shedding strategy proposed in this paper aims to fully consider multiple types of load shedding-related factors while minimizing the adverse effects of load shedding. In this section, the frequency regulation model of islanded microgrid is first described. Then, the relevant factors of integrated load shedding are introduced, and on this basis, the differences between the proposed integrated load shedding mode and the traditional load shedding mode are described. Then, the objective function of integrated load shedding is introduced, and finally, the operational constraints of the islanded microgrid system are explained.

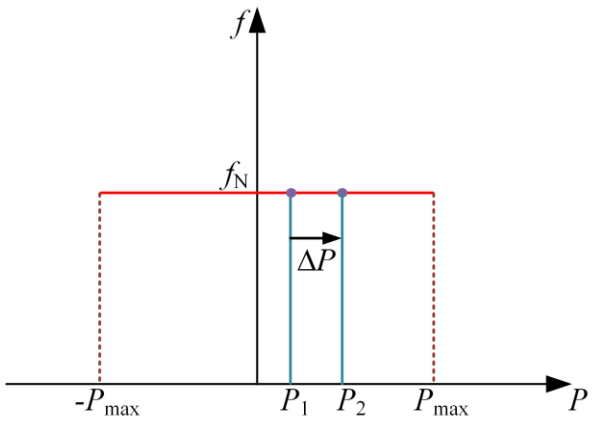

Fig. 1. V/f Operation Principle of BESS

A. Islanded Microgrid Frequency Regulation Model

In islanded operation mode, microgrids dominated by renewable energy lack the frequency and voltage support of the main grid. The frequency stability of the microgrid relies on the regulation of its DGs and battery energy storage systems (BESS). With its fast response characteristics and stable power supply capabilities, BESS can charge/discharge in real-time according to the system's actual power demand, effectively addressing the insufficient regulation capacity caused by the intermittent output of DGs. In the islanded microgrid model constructed in this paper, BESS is connected to the system through grid-forming mode inverters and uses V/f control to maintain stable voltage and frequency in the islanded microgrid. DGs operating in grid-following mode provide power support to the islanded microgrid system using PQ control under stable voltage and frequency support, working together with BESS in grid-forming mode to maintain system power balance. The V/f operation principle of BESS is shown in Fig. 1. As indicated in Fig. 1, under rated frequency f_N, when the system experiences a power deficit ΔP, BESS adjusts its output power to compensate for the deficit, thereby maintaining system frequency stability. When the maximum output power of DGs and BESS in the islanded microgrid is still insufficient to meet the load demand, load shedding through underfrequency load shedding becomes inevitable.

B. Factors Related to Load Shedding

1) Load Frequency Characteristics

The active and reactive power absorbed by loads in the power system varies with changes in frequency and voltage, which are called the static characteristics of the load voltage and frequency. To more accurately calculate the frequency change rate and power shortage of an islanded microgrid during underfrequency load shedding, it is necessary to consider the static frequency characteristics of the load. Considering the strong coupling between the system frequency and the active power, the load frequency characteristic model can be expressed as [27]:

$$P_L = \varepsilon_0 P_{L0} + \varepsilon_1 P_{L0}(f/f_0) + \varepsilon_2 P_{L0}(f/f_0)^2 + \cdots + \varepsilon_n P_{L0}(f/f_0)^n \quad (1)$$

This article has been accepted for publication in a future issue of this journal, but has not been fully edited. Content may change prior to final publication.
Citation information: DOI: 10.1109/TSG.2025.3586757, IEEE Transactions on Smart Grid

Where P_L represents the active power absorbed by the load at frequency f; P_{L0} represents the rated active power of the load; ε_n represents the proportion of load proportional to the n th power of system frequency in P_{L0}.

Differentiate the above equation and convert it into per unit form to obtain:

$$K_L = dP_L^* / df^* = \varepsilon_1 + 2\varepsilon_2 f^* + \cdots + n\varepsilon_n f^{*(n-1)} \tag{2}$$

Where K_L represents the frequency regulation effect coefficient of the load.

When the system frequency changes, different loads have different frequency regulation effects, as shown in Fig. 2 (a). From Fig. 2 (a), it can be seen that loads with large coefficients of the frequency regulation effect result in more significant frequency changes. When the system frequency decreases from f_0 to f, the load with a larger frequency regulation effect coefficient absorbs a greater amount ΔP_{L1} of power reduction, which can better alleviate the power balance burden of the system. Therefore, when the system frequency decreases and triggers underfrequency load shedding action, priority should be given to cutting off loads with small frequency regulation effect coefficients and retaining loads with large regulation effect coefficients. The frequency recovery curves of the system after different loads are cut off during underfrequency load shedding are shown in Fig. 2 (b), it can be seen from Fig. 2 (b) that when the frequency recovery is faster, the difference between the peak and valley values of the system frequency is smaller ($\left|f_2^{\wedge} - f_2^{\vee}\right| < \left|f_1^{\wedge} - f_1^{\vee}\right|$). Therefore, the frequency regulation effect coefficient of the load during underfrequency load shedding can be represented by the amplitude of system frequency fluctuations.

2) Load Shedding Cost

Typically, loads are divided into three categories: primary loads, secondary loads, and tertiary loads. However, this simple classification method ignores the differences in the demands of electricity users for different types of loads at different time scales. In this paper, a load cost factor is used to measure the load shedding priorities at different times. The cost coefficient $F_{i,t}$ of load i at time t is:

$$F_{i,t} = C_{i,t}\omega h_i \tag{3}$$

where $C_{i,t}$ represents the time-varying demand coefficient for load i at time t, which is determined by the type of load. In this paper, loads are divided into three categories, industrial, commercial and residential [28], and the demand degrees of these types of loads are different. ω represents the weight of the load level, which is divided into levels I, II and III according to the social and economic losses caused by the load power loss, corresponding to 100, 10 and 1, respectively [29]. h_i represents the coefficient of load shedding loss.

During underfrequency load shedding, on the basis of the magnitude of the load cost coefficient, priority is given to cutting off loads with low cost coefficients to ensure minimal losses during the shedding process.

3) Load Characteristics under Three-phase Unbalance

With the rapid popularization and development of microgrid, hybrid microgrids formed by the fusion of three-phase source-load-storage and multiple-phase-sequence single-phase source-load-storage are widely studied. Due to the presence of many single-phase devices, there may be a three-phase power unbalance in the interconnection line of the microgrid during operation, which will increase system losses and reduce the power quality of the microgrid and may even prevent the system from operating normally. With three-phase power as the calculation variable, the formula for calculating the three-phase unbalance degree of an islanded microgrid is as follows [30]:

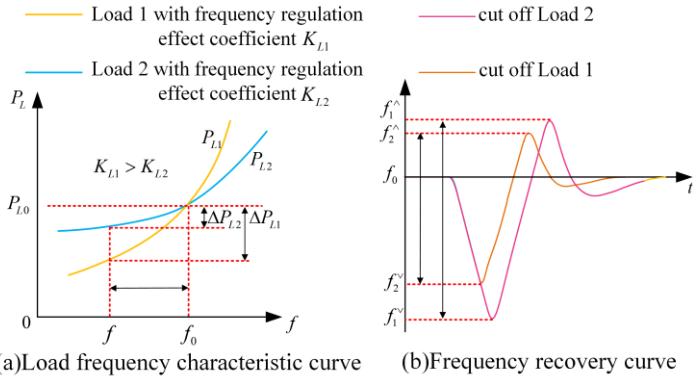

(a)Load frequency characteristic curve (b)Frequency recovery curve

Fig. 2. Load frequency characteristic curves

$$Unbalance = \frac{I_2}{I_1} = \frac{S_{L2}}{S_L} \tag{4}$$

$$\begin{cases} S_L = \sqrt{\left(P_A + P_B + P_C\right)^2 + \left(Q_A + Q_B + Q_C\right)^2} \\ S_{L2} = \sqrt{P_{L2}^2 + Q_{L2}^2} \\ P_{L2} = \dfrac{1}{2}\left(2P_A - P_B + \sqrt{3}Q_B - P_C - \sqrt{3}Q_C\right) \\ Q_{L2} = -\dfrac{1}{2}\left(2Q_A - Q_B - \sqrt{3}P_B + \sqrt{3}P_C - Q_C\right) \end{cases} \tag{5}$$

Where I_1 is the root mean square value of the positive sequence component of the three-phase current; I_2 is the root mean square value of the negative sequence component of the three-phase current; P_A, P_B, P_C and Q_A, Q_B, Q_C are respectively three-phase active power and reactive power; S_L, S_{L2} and P_{L2}, Q_{L2} are the positive and negative sequence apparent power, as well as the negative sequence active and reactive power, respectively.

When studying the underfrequency load shedding problem for islanded microgrid systems, it is necessary to consider the three-phase unbalance characteristics of the load during the load shedding process. To restore the system frequency to a safe range, it is necessary to minimize the three-phase unbalance degree of the microgrid system during load shedding.

C. Basis of Integrated Load Shedding

From the analysis in the previous section, it can be concluded that the frequency regulation effect of the load, the cost of load shedding, and the three-phase unbalance degree of the load are the load shedding-related factors that must be considered during the shedding process. In traditional research, to fully consider the impact of these factors, researchers usually construct a load evaluation model to measure the contribution of these factors to the system frequency recovery during the load shedding process, and then based on this contribution, construct an underfrequency

This article has been accepted for publication in a future issue of this journal, but has not been fully edited. Content may change prior to final publication.
Citation information: DOI: 10.1109/TSG.2025.3586757, IEEE Transactions on Smart Grid

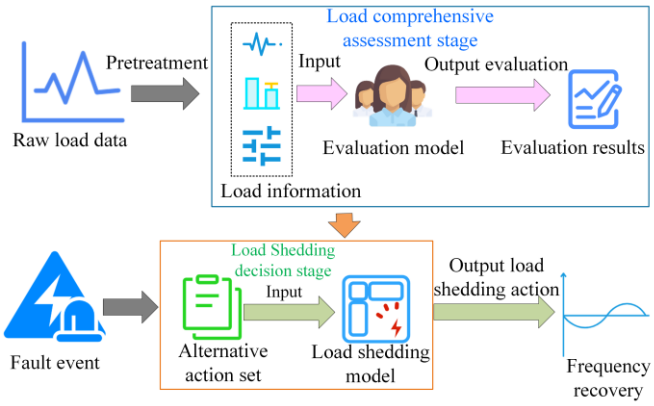

(a) Assessment of the load shedding mode of decision separation

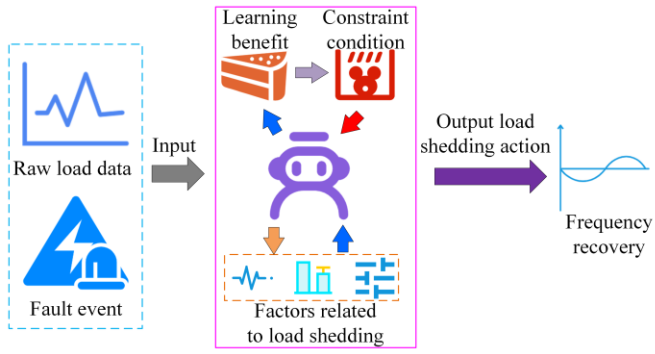

(b) Integrated load shedding mode

Fig. 3. Comparison of different load shedding modes

load shedding control set for load shedding actions. This emergency load shedding control mode of evaluation and load shedding separation is shown in Fig. 3 (a). From Fig. 3 (a), it can be seen that the comprehensive evaluation of the load and the decision to reduce the load are relatively independent stages, and the generation of load shedding decisions depends on the real-time comprehensive load evaluation results. When a fault event occurs, it is first necessary to conduct a comprehensive evaluation of the load information through the evaluation model. Then, based on the load evaluation results, the load shedding model is used to generate online load shedding strategies. The process of comprehensive load evaluation delays the response speed of the decision to reduce the load, impacting the control effect of the entire underfrequency load shedding action. The proposed integrated load shedding strategy uses the DRL method to merge the two relatively independent stages into one, forming an end-to-end integrated load shedding mode, as shown in Fig. 3 (b).

In the integrated load shedding mode, all the fault data and the original load information are directly input into the intelligent agent as the decision-making basis for load shedding. The load evaluation stage is incorporated into the training process of the agent by using the mechanism linked to the agent's learning benefits so that the agent can independently mine the mapping relationship between load information and decision-making. The trained agent can directly generate online decisions based on the real-time load data and system state information under the fault event, without independent evaluation steps to evaluate the contribution of the load, and thus avoid the action response delay caused by the step-by-step execution of evaluation and decision.

D. Integrated Load Shedding Objective Function

According to the analysis in sections A and B, the proposed integrated underfrequency load shedding model requires that the system frequency of the islanded microgrid be restored to the normal level with the minimum load shedding cost, and the three-phase system unbalance caused by the fault or underfrequency load shedding should be minimized considering the load frequency regulation effect and load importance. Therefore, the frequency fluctuation amplitude, cost and three-phase unbalance degree of the system in the load shedding process are simultaneously minimized according to the objective function of underfrequency load shedding:

$$\begin{cases} \min\left(f^{\wedge}-f^{\vee}\right) \\ \min g=\sum_{i=1}^{m}F_{i,t}P_{i,t}^{cut} \\ \min Unbalance \end{cases} \tag{6}$$

where $f^{\wedge}$ and $f^{\vee}$ represent the peak and valley values, respectively, in the frequency recovery process of the islanded microgrid; m represents the number of loads in the islanded microgrid system; and $P_{i,t}^{cut}$ represents the amount of load i removed at time t.

E. Constraint Condition

To ensure that underfrequency load shedding meets the operation requirements of islanded microgrid systems, the following constraints should be met:

1) Power Flow Constraint

$$\begin{cases} P_{i,t}-U_{i,t}\sum_{j\in i}U_{j,t}(\mathrm{G}_{ij}\cos\theta_{ij,t}+B_{ij}\sin\theta_{ij,t})=0 \\ Q_{i,t}-U_{i,t}\sum_{j\in i}U_{j,t}(\mathrm{G}_{ij}\cos\theta_{ij,t}-B_{ij}\sin\theta_{ij,t})=0 \end{cases} \tag{7}$$

where $P_{i,t}$ and $Q_{i,t}$ represent the active power and reactive power of node i, respectively, at time t; $U_{i,t}$ and $U_{j,t}$ represent the voltage amplitudes of nodes i and j, respectively, at time t; $\theta_{ij,t}$ represents the voltage phase angle difference of nodes i and j at time t; and G_{ij} and B_{ij} represent the conductance and susceptance, respectively, between nodes i and j.

2) Load Shedding Constraint

$$P_i^{cut,\min}\le P_i^{cut}\le P_i^{cut,\max} \tag{8}$$

where $P_i^{cut,\min}$ and $P_i^{cut,\max}$ represent the minimum and maximum load shedding, respectively, of node i.

3) Frequency Constraint

$$f^{\min}\le f\le f^{\max} \tag{9}$$

where $f^{\min}$ and $f^{\max}$ represent the minimum and maximum frequencies allowed for normal operation of the system, respectively.

4) Three-phase Unbalance Degree Constraint [31]

$$Unbalance_t\le 15\% \tag{10}$$

This article has been accepted for publication in a future issue of this journal, but has not been fully edited. Content may change prior to final publication.
Citation information: DOI: 10.1109/TSG.2025.3586757, IEEE Transactions on Smart Grid

III. Markov Decision Modeling for Integrated Underfrequency Load Shedding

The action determined for integrated load shedding in the islanded microgrid is related only to the current state of the microgrid and has nothing to do with the action and state corresponding to the previous sequence time. This means that the decision problem for underfrequency load shedding satisfies the Markov property and can be described as a Markov decision process. Under the framework of reinforcement learning, the MDP is a process in which agents and the environment constantly interact to learn and seek the optimal strategy to obtain the maximum return; which is mainly composed of (S, A, R, P, γ) [32].

In this paper, the operating state of the islanded microgrid is the environment, and the amount of each load to shed in the microgrid is the action. To find the optimal load shedding strategy for the islanded microgrid, the state space, action space, and reward function are set as follows:

1) State Space s

The state space should reflect the operation characteristics of the islanded microgrid as well as possible. Therefore, the output P_t^{DG} of the DG unit, real-time power P_t^L of the load, real-time frequency f_t of the microgrid, and frequency change rate ROCOF_t are selected. For any time t, the state is expressed as:

$$s_t = \left\{ P_t^{DG}, P_t^L, f_t, \mathrm{ROCOF}_t \right\} \tag{11}$$

2) Action Space a

The action space is the relevant decision quantity in the load shedding model. In this paper, the shedding power P_i^{cut} of the load at node i is considered the action; then, the action space a_t of the islanded microgrid system at time t can be expressed as:

$$a_t = \left\{ P_{i,t}^{cut} \right\} \tag{12}$$

3) Reward r

The goal of the proposed integrated underfrequency load shedding strategy is to ensure that the frequency of the islanded microgrid is restored to the normal operating level with the minimum frequency fluctuation amplitude and load shedding cost, while the three-phase unbalance of the system is as small as possible. In addition, the environment should include the system operation constraints of equations (7)-(10) when giving feedback rewards to the agent. Therefore, the reward value for the agent at time t is expressed as:

$$r_t = -\alpha_1 \left(f^{\wedge} - f^{\vee} \right) - \alpha_2 \sum_{i=1}^{m} F_{i,t} P_i^{cut} - \alpha_3 Unbalance_t + \chi_t \tag{13}$$

where α_1, α_2 and α_3 represent the coefficient factors of the frequency fluctuation amplitude, load shedding cost and three-phase unbalance degree of the system in the reward function, respectively, and where χ_t represents the punishment when the agent's decision cannot meet the operational constraints of the islanded microgrid.

IV. Integrated Underfrequency Load Shedding Strategy Based on DBR-SD3

A. SD3

The proposed SD3 is implemented on the TD3 framework. TD3 is a DRL method designed specifically for dealing with high-dimensional continuous action spaces. It was developed from the DDPG algorithm and has stronger stability and generalization performance [23]. By introducing the clipping double-Q learning mechanism in TD3, the problem of overestimating the Q value in parameter updating is limited to a great extent. However, this mechanism may lead to an underestimation of the Q value, which may affect the performance of the method. Therefore, a new SD3 method based on TD3 is designed in this paper. By introducing softmax into TD3, this method not only avoids the overestimation problem for the DDPG but also effectively alleviates the influence of underestimation bias in TD3 and accurately estimates the value function. $\mathrm{softmax}\left(Q'\left(s_{t+1}^b, a_{t+1}^b\right)\right)$ is obtained via importance sampling. The specific formula is as follows:

$$\mathrm{softmax}\left(Q'\left(s_{t+1}^b, a_{t+1}^b\right)\right) = \frac{\mathbb{E}\left[\dfrac{\exp\left(\beta Q'\left(s_{t+1}^b, a_{t+1}^b\right)\right) Q'\left(s_{t+1}^b, a_{t+1}^b\right)}{p\left(a_{t+1}^b\right)}\right]}{\mathbb{E}\left[\dfrac{\exp\left(\beta Q'\left(s_{t+1}^b, a_{t+1}^b\right)\right)}{p\left(a_{t+1}^b\right)}\right]} \tag{14}$$

where $Q'\left(s_{t+1}^b, a_{t+1}^b\right)$ represents the smaller Q value estimated by the two critic networks; the probability density function $p\left(a_{t+1}^b\right)$ satisfies the Gaussian distribution; and β indicates the operation parameter of $\mathrm{softmax}$. After introducing the $\mathrm{softmax}$ operator, the formula for calculating the target Q value y_t^b is as follows:

$$y_t^b = r_t^b + \mathrm{softmax}\left(Q'\left(s_{t+1}^b, a_{t+1}^b\right)\right) \tag{15}$$

B. Dual-Replay Buffer Mechanism

TD3 stores exploration data by setting up a playback buffer and randomly extracts small batches of data for training. However, random sampling may result in uneven data quality, which affects training efficiency and convergence speed. In this context, this paper presents a DBR mechanism based on the TD3 framework, which classifies and stores experience data according to their importance and extracts parts of the experience data from two buffers as training samples according to different probabilities during training.

Under DBR, experience data are stored in buffers $\mathcal{D}_1$ and $\mathcal{D}_2$ according to their immediate reward r_t. Considering the time-ductility of reinforcement learning reward feedback, a temporary experience playback buffer $\mathcal{D}_0$ with a capacity of M is set up to store M adjacent experience data values. When the

This article has been accepted for publication in a future issue of this journal, but has not been fully edited. Content may change prior to final publication.
Citation information: DOI: 10.1109/TSG.2025.3586757, IEEE Transactions on Smart Grid

amount of stored experience data in $\mathcal{D}_0$ reaches the maximum capacity, the instant reward mean $\bar{r}$ of all experience data in $\mathcal{D}_0$ is calculated, and the data in $\mathcal{D}_0$ are judged according to the order of storage time. If the reward value r_t is greater than or equal to $\bar{r}$, it is stored in buffer $\mathcal{D}_1$; otherwise, it is stored in buffer $\mathcal{D}_2$. The new experience data are then stored in $\mathcal{D}_0$ until the entire learning process is complete. Finally, the remaining experience data in $\mathcal{D}_0$ are stored in $\mathcal{D}_1$ and $\mathcal{D}_2$ according to the reward mean $\bar{r}$, and $\mathcal{D}_0$ is cleared.

According to the empirical storage classification rule, the value of the sample data stored in $\mathcal{D}_1$ is greater than that of the data in $\mathcal{D}_2$. The training process aims to extract more valuable experiences from $\mathcal{D}_1$ with a higher probability, so the preferred experience replay method is used for buffer $\mathcal{D}_1$. Moreover, to ensure the diversity of sample data, sample data with small immediate rewards and low importance should also be extracted from $\mathcal{D}_2$ in small batches. The specific sampling method is as follows:

$$\begin{cases} M_1 = \eta m \\ M_2 = (1-\eta) m \end{cases} \tag{16}$$

where M_1 and M_2 represent the numbers of sample data values extracted from buffers $\mathcal{D}_1$ and $\mathcal{D}_2$, respectively; $\eta \in [0,1]$ represents the extraction rate of samples from buffer $\mathcal{D}_1$; and m indicates the number of small-batch samples.

Priority experience playback means preferentially extracting experience data with higher values in the buffer, and the priority p of the sample data is measured by the temporal difference error; for example, the priority of the k th sample is as follows:

$$p_k = \left| y_t^k - Q_w\left(s_t^k, a_t^k\right) \right| \tag{17}$$

The probability that the k th sample is chosen is:

$$p_k' = \frac{p_k}{\sum_{n=1}^{M_1} p_n} \tag{18}$$

C. Integrated Load Shedding Strategy Framework

The proposed integrated underfrequency load shedding strategy for a microgrid based on DBR-SD3 is divided into two parts: offline learning and online application.

The offline training steps for DBR-SD3 are as follows:

Randomly initialize the parameters of the two Critic networks and the Actor network: w_1, w_2, θ.
Initialize the target network parameters: $w_1' \leftarrow w_1$, $w_2' \leftarrow w_2$, $\theta' \leftarrow \theta$.
for number of rounds =1 : M^{train} **do**
  Initialize search noise $\mathcal{N}$
  Obtain the initial environment state s_0 from the islanded microgrid system
  for t=1 : $T_{\max}$ **do**
    for n=1,2 **do**
  Select actions and add noise according to state s_t
  Perform action a_t and get reward r_t and the next state s_{t+1}
  Store the experience data in the temporary buffer $\mathcal{D}_0$, and store the experience data in buffers $\mathcal{D}_1$ and $\mathcal{D}_2$ according to the sorting storage rules in section IV-C
  Calculate the temporal difference error of the sample drawn from $\mathcal{D}_1$ and update the sample priority p_k
  Calculate the next time action a_{t+1} according to the Critic network
  Calculate the target Q value y_t for each sample using softmax
  Update the Critic network parameter w
  Update the Actor network parameters θ every d steps
  Soft-update the target network parameters w' and θ'
    end for
  end for
end for

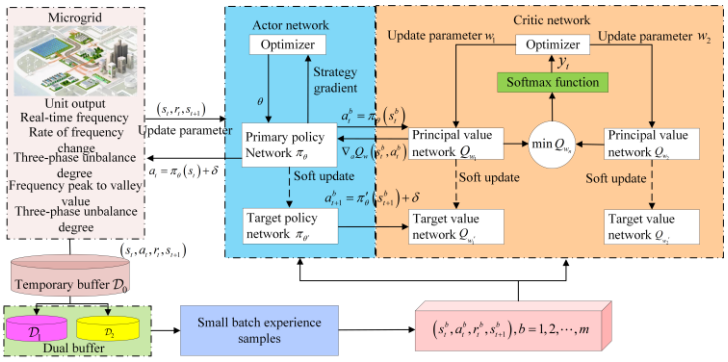

Fig. 4. Integrated load shedding strategy framework

After offline training is complete, the parameters of the integrated load shedding model are saved. In online applications, the current state value of the islanded microgrid system plus the random error value is input to the Actor network as a comprehensive state; after full learning, DBR-SD3 directly generates the optimal integrated load shedding decision. The integrated load shedding strategy framework based on DBR-SD3 is shown in Fig. 4.

V. Simulation Analysis

To verify the feasibility and effectiveness of the proposed underfrequency load shedding strategy, an islanded microgrid system model based on an improved IEEE 37-bus system is built on the MATLAB/Simulink simulation platform, as shown in Fig. 5. The model consists of 9 DGs, 6 battery energy storage (BES) systems, and 19 loads. BES1-BES6 operates in the grid-forming mode, while DG1-DG9 operates in the grid-following mode. Among them, LD1-10 are three-phase loads, and LD11-19 are single-phase loads. According to the social and economic losses caused by load power loss, the loads are divided into levels I, II, and III based on their importance. Additionally, according to the type of electricity, the loads are classified into industrial loads, commercial loads, and residential loads [34]. The DG and energy storage output information are shown in TABLE I, the load grades and load types are shown in TABLE II, and the load demand degrees at different times are shown in Fig. 6. In this paper, when implementing the underfrequency load shedding strategy, the communication transmission delay is set to 10 ms, the relay startup and underfrequency load shedding delays are set to 10 ms [35], and the trigger threshold of the load shedding action is set to 49.5 Hz [36].

This article has been accepted for publication in a future issue of this journal, but has not been fully edited. Content may change prior to final publication.
Citation information: DOI: 10.1109/TSG.2025.3586757, IEEE Transactions on Smart Grid

A. Test Environment and Parameter Setting

The proposed DBR-SD3 consists of an Actor network and two Critic networks, both of which are made of four fully connected neural networks with two hidden layers: the number of neurons in the first hidden layer is 400, and the number of neurons in the second hidden layer is 300. The activation function is a rectified linear unit (ReLU). The other hyperparameters used during DBR-SD3 training are shown in TABLE III.

On the basis of the above settings, the Python language is used to implement the DRL method on the TensorFlow framework. All tests are conducted on a 3.40 GHz Intel(R) Core (TM) i5-7500 CPU.

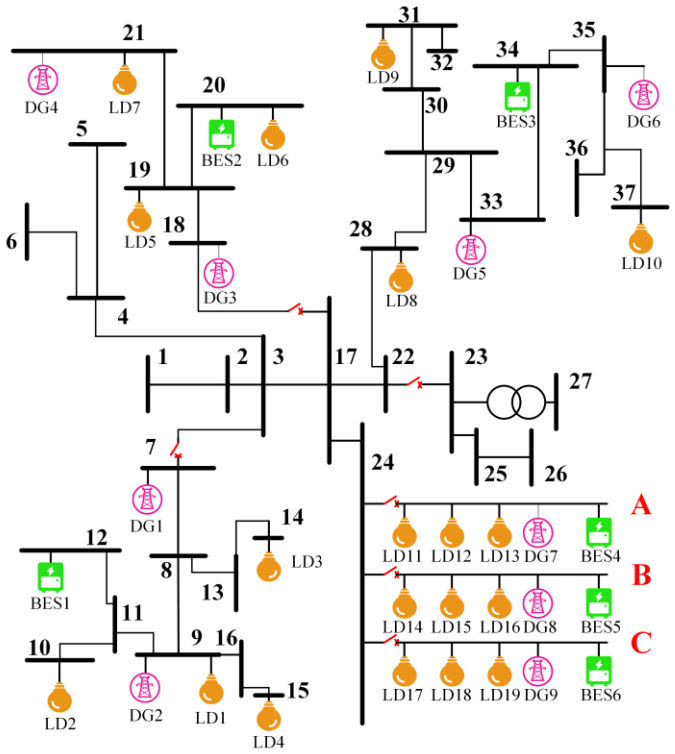

Fig. 5. Improved IEEE 37-bus island microgrid system model

TABLE I
DG AND ENERGY STORAGE CONFIGURATION INFORMATION

Name	Access location	Output (kW)	Name	Access location	Output (kW)
DG1	Bus 7	100	DG9	Bus 24-C	35
DG2	Bus 9	150	BES1	Bus 12	75
DG3	Bus 18	70	BES2	Bus 20	25
DG4	Bus 21	90	BES3	Bus 34	100
DG5	Bus 33	65	BES4	Bus 24-A	20
DG6	Bus 35	80	BES5	Bus 24-B	40
DG7	Bus 24-A	30	BES6	Bus 24-C	30
DG8	Bus 24-B	25			

TABLE II
LOAD DATA INFORMATION

Load	Priority	P^L (kW)	h(\$/kWh)	$P^{cut,\max}$ (kW)	Load type
LD1	III	100	0.75	60	residential
LD2	II	70	1.26	35	commercial
LD3	I	90	3.03	30	industrial
LD4	III	50	0.62	30	commercial
LD5	II	75	1.28	35	industrial
LD6	I	52.5	2.98	15	commercial
LD7	III	50	0.63	30	commercial
LD8	III	110	0.68	80	industrial
LD9	I	82.2	3.01	40	residential
LD10	II	75	1.24	40	residential
LD11	III	20	0.55	10	commercial
LD12	I	10	2.46	5	residential
LD13	III	20.4	0.58	15	residential
LD14	II	25	1.16	10	industrial
LD15	III	16	0.54	12	commercial
LD16	I	19.5	2.55	8	commercial
LD17	III	20	0.51	10	residential
LD18	III	20	0.52	10	commercial
LD19	III	25.4	0.61	15	industrial

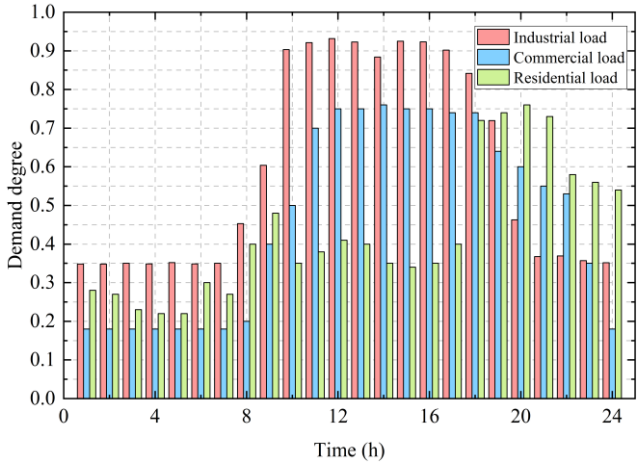

Fig. 6. Different types of load demand

TABLE III
PARAMETER SETTINGS

Parameter	Value	Parameter	Value
Discount factor γ	0.95	Number of small-batch samples m	128
Soft update coefficient τ	0.001	Training steps per round $T_{\max}$	200
Critic network learning rate μ_w	0.003	Extraction probability η	0.9
Actor network learning rate μ_θ	0.0003	Maximum number of iterations	2000
Playback buffer capacity $\mathcal{D}_1$	50000	Network latency update interval d	2
Playback buffer capacity $\mathcal{D}_2$	50000	Extraction rate η of buffer $\mathcal{D}_1$	0.9
Action noise variance σ	0.03	Soft update coefficient τ	0.005

B. Training Performance Analysis

To simulate the frequency disturbance of the islanded microgrid system, the fault scenario is set as follows: under different load demand degrees, a DG or BES is randomly selected to exit operation to cause a decrease in system frequency. To simulate different operating states of the system, the loads are randomly set to 95% -105% of the initialization level, generating a total of 1080 training scenarios. The duration of a single training episode is set to 2 seconds, and the data collection resolution is 0.01 seconds. The proposed DBR-SD3 and other DRL methods are compared by using the above training scenarios, and the results are shown in Fig. 7.

A Specific analysis of Fig. 7 shows that the average reward of the proposed DBR-SD3 is close to optimal after approximately 400 training rounds. Compared with TD3/DDPG/DQN, DBR-SD3 converges 200/900/1000 rounds earlier, indicating that the speed of DBR-SD3 learning the optimal load shedding control strategy is about 1.5/3.25/3.5 times that of TD3/DDPG/DQN, respectively. In addition, the average reward obtained when DBR-SD3 converges is greater than those of TD3/DDPG/DQN, the average

This article has been accepted for publication in a future issue of this journal, but has not been fully edited. Content may change prior to final publication.
Citation information: DOI: 10.1109/TSG.2025.3586757, IEEE Transactions on Smart Grid

rewards for TD3/DDPG/DQN convergence are -304.1/-385.55/-604.88, respectively. The proposed DBR-SD3 has improved by 31.46%/45.94%/65.54% on this basis, reaching -208.42. This is mainly because the strategy proposed in this paper introduces softmax and the dual-buffer replay mechanism into TD3, greatly improving the learning speed and convergence performance of the agent and enabling the agent to adaptively learn more stable control strategies. Specifically, the faster convergence speed of DBR-SD3 stems from its introduced DBR mechanism, which dynamically classifies and stores training samples by evaluating their immediate reward values. This mechanism enhances the agent's utilization efficiency of high-value samples during training, reduces interference from low-reward samples on policy learning, and enables the agent to learn the optimal strategy along a more efficient convergence trajectory. The higher reward value achieved by DBR-SD3 at convergence is attributed to the integration of the softmax mechanism into TD3. This integration not only effectively suppresses the Q-value overestimation issue inherent in DDPG but also mitigates the Q-value underestimation problem caused by TD3's conservative estimation. By reducing Q-value estimation bias and improving the accuracy of value function estimation, this mechanism allows the agent to precisely identify and learn high-return strategies, thereby enhancing the quality of the final converged policy.

The offline training times of the four DRL methods are shown in Table IV. From Table IV, it is evident that DQN requires the shortest offline training time. This is mainly because DQN only requires training one deep neural network (DNN), resulting in fewer parameters to fit and thus less time spent on offline training. However, its reliance on discrete action spaces limits its ability to search for optimal strategies, leading to inferior policy quality compared to the other three DRL methods, as validated in Fig. 7. Among the remaining three DRL methods, DBR-SD3 exhibits the shortest offline training time. This is due to the introduced softmax mechanism optimizing the agent's policy update direction and the DBR mechanism improving the utilization efficiency of high-quality samples, reducing its training time by 10.05% and 7.67% compared to TD3 and DDPG, respectively.

Overall, the above comparison demonstrates the superiority of DBR-SD3 proposed in this paper in offline training of load shedding control in islanded microgrids, with the best overall performance in terms of learning speed and learning quality.

C. Superiority Analysis of Load Shedding Strategies

To verify the superiority of the proposed strategy compared with other underfrequency load shedding strategies, the following typical fault scenario is set: BES3 exits operation at 8:00 because of a fault, and the load level is 100%. Owing to the loss of output support from a high-power energy storage system in the islanded microgrid system, the frequency begins to decrease, and emergency load shedding control must be implemented immediately to restore the system to normal operation. In this scenario, the integrated load shedding strategy proposed in this paper is analyzed and compared with the other three load shedding strategies. The specific settings for the comparison strategies are as follows:

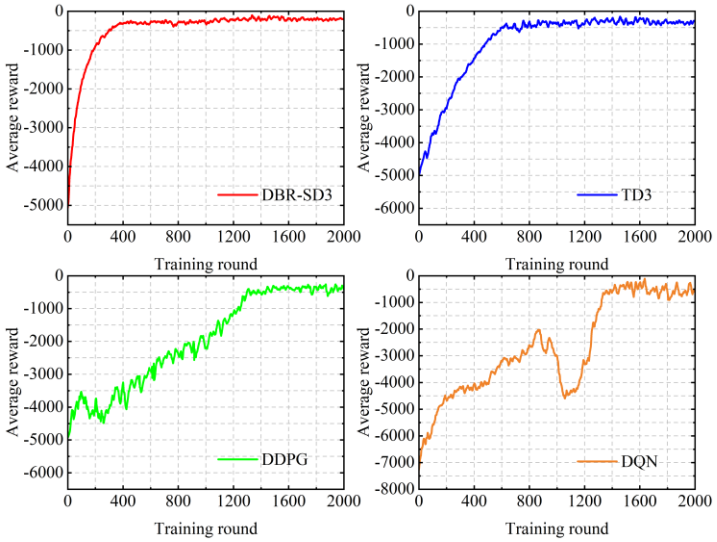

Fig. 7. Comparison of the training processes of the four DRL methods

Table IV
COMPARISON OF TRAINING TIME OF FOUR DRL METHODS

Method	DBR-SD3	TD3	DDPG	DQN
Training time/ h	7.34	8.16	7.95	6.98

Strategy 1: The integrated load shedding strategy proposed in this paper;

Strategy 2: The adaptive load shedding scheme based on MPC in [10];

Strategy 3: The emergency load shedding strategy based on DDPG in [20];

Strategy 4: The underfrequency load shedding strategy based on a DQN in [26].

(1) Comparison of Load Shedding Compositions

The composition of load shedding after the four load shedding strategies are implemented is shown in Fig. 8 (a-e).

As can be seen from Fig. 8(a), strategy 1 achieves the smallest load shedding amount among the four strategies, only requiring the removal of 102kW of loads. Compared with strategies 2, 3, and 4, the load shedding amount is reduced by 5.12%, 3.32%, and 4.67%, respectively. This is because strategy 1 fully considers the frequency regulation effect of the load during load shedding. By prioritizing the removal of loads with smaller frequency regulation effect coefficients, the system frequency can return to normal more quickly, resulting in the least amount of load shedding. Additionally, none of the four strategies shed levels I or II loads, ensuring the continuous power supply of important loads during the load shedding period of the islanded microgrid system. Further analysis of the specific load shedding targets under each strategy shows that parts of the loads on LD4, LD7, LD11, LD13, LD15, LD17, LD18, and LD19 are removed in strategies 2 and 3, as shown in Fig. 8(b-e). However, neither of these strategies consider the three-phase power unbalance caused by single-phase loads during the load shedding process, which may make the islanded microgrid unable to meet normal operation requirements after load shedding. Strategy 4 considers the problem of load shedding cost and three-phase load unbalance. In the process of load shedding, the virtual combination and evaluation of each single-phase load are first carried out, and then a group of load combinations with the least unbalance are removed on LD13, LD15, and LD19. It is worth noting that the above three strategies do not consider the

This article has been accepted for publication in a future issue of this journal, but has not been fully edited. Content may change prior to final publication.
Citation information: DOI: 10.1109/TSG.2025.3586757, IEEE Transactions on Smart Grid

user's demand preferences for different load types and fail to comprehensively evaluate the load. From Fig. 8(a), it can be observed that strategies 2, 3, and 4 all shed some industrial loads with relatively high demand during the load shedding process, accounting for 12.09%, 14.22%, and 21.50% of the total load shedding amount respectively. In contrast, strategy 1 considers multiclass load-related factors including relative electricity demand, avoiding the removal of high-demand load types and thereby minimizing the impact of load shedding on users' demand. In summary, compared with strategies 2, 3, and 4, strategy 1 not only minimizes the load shedding amount but also ensures the continuous power supply of important loads and loads with high user demand, achieving a more ideal load shedding effect.

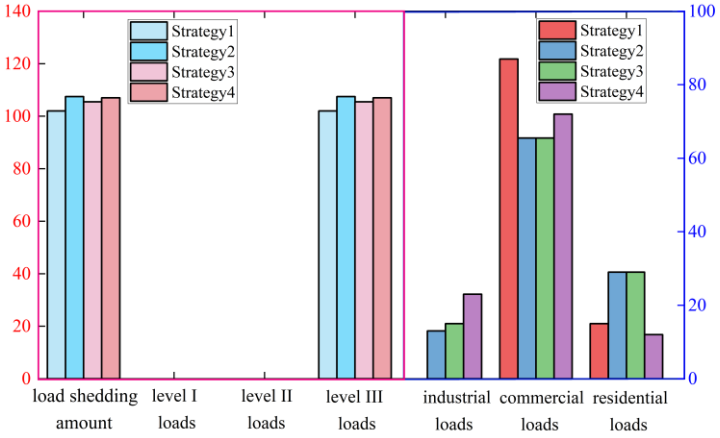

(a) Different types of load shedding amount under four strategies

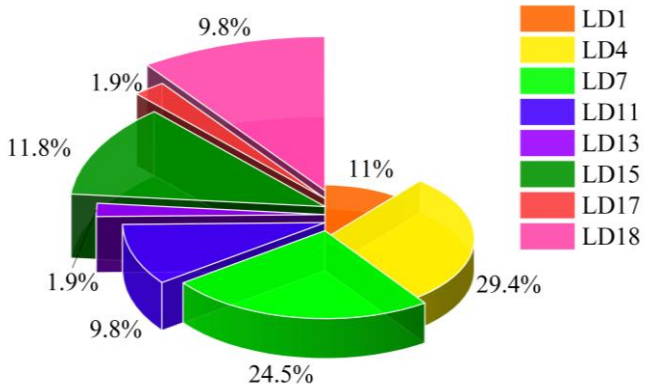

(b) Load shedding under strategy 1

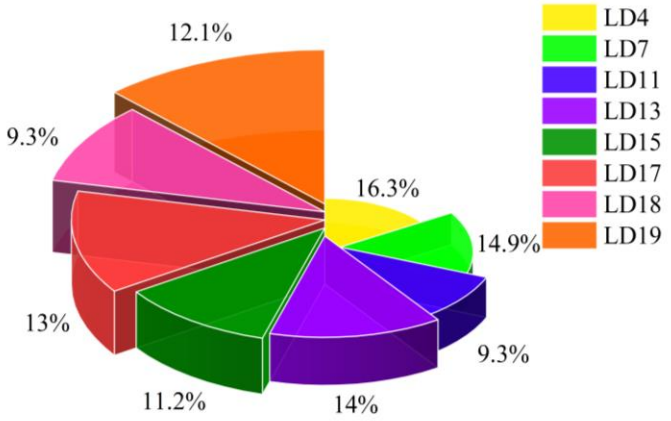

(c) Load shedding under strategy 2

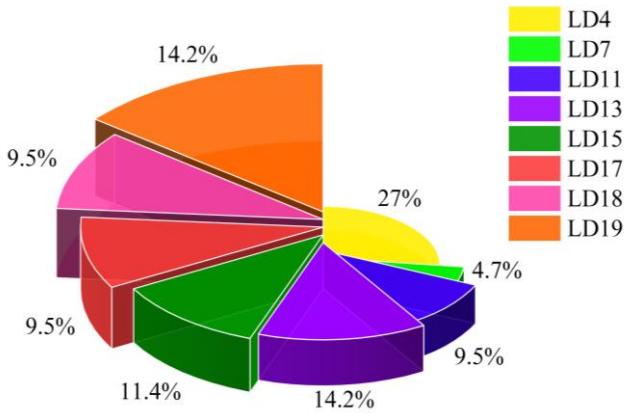

(d) Load shedding under strategy 3

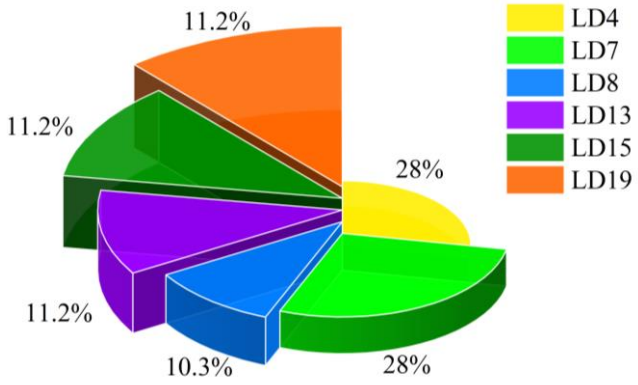

(e) Load shedding under strategy 4

Fig. 8. Comparison of load shedding under different strategies

TABLE V
COMPARISON OF LOAD SHEDDING COSTS UNDER DIFFERENT STRATEGIES

Index	Strategy 1	Strategy 2	Strategy 3	Strategy 4
Load shedding cost g /$	14.49	17.53	17.24	18.24

(2) Comparison of Load Shedding Costs

A comparison of the load shedding costs for each strategy is shown in TABLE V.

TABLE V shows that the load shedding cost of strategy 4 is the highest, 4.05% and 5.8% higher than those of strategies 2 and 3, respectively. This is because strategy 4 considers the impact of three-phase unbalance in the system and is constrained by a certain amount of load shedding distribution during the shedding process. It is necessary to cut off a virtual combination of approximately balanced loads in the three phases. Furthermore, although strategy 1 also considers the impact of the three-phase unbalance in the system, its load shedding process also considers the demand differences of different types of loads. It eliminates the batch of loads with the lowest cost coefficient in the fault scenario so that the load shedding cost of strategy 1 is still the lowest among the four strategies; it is 17.34%, 15.95%, and 20.56% lower than those of strategies 2, 3, and 4, respectively.

(3) Comparison of the Frequency Recovery Effects

To better compare the frequency recovery effect of the islanded microgrid system before and after load shedding, the failure occurrence time is set to $t = 1$ s. The frequency recovery waveforms of the islanded microgrid system after load shedding under the four strategies are shown in Fig. 9. The online calculation time t_{on}, system frequency recovery time t_{sum} and

This article has been accepted for publication in a future issue of this journal, but has not been fully edited. Content may change prior to final publication.
Citation information: DOI: 10.1109/TSG.2025.3586757, IEEE Transactions on Smart Grid

frequency fluctuation amplitude Δf under each load shedding strategy are shown in Table VI.

According to the analysis of Fig. 9, when a power deficit occurs at $t=1$s in the islanded microgrid system due to BES 3 exits operation, the four strategies reduce the load demand by cutting off part of the load to restore the system frequency to a normal level.

As can be seen from Table VI, the online calculation time consumed for strategy 2 is significantly higher than the other strategies. This is mainly because strategy 2 is a load shedding strategy based on MPC, which needs to solve the optimization model online and has a heavier computational burden. In contrast, strategies 1, 3, and 4 are all DRL-based methods, which enable the agent to acquire rich decision-making experience through offline training in the early stage. In actual operation, the trained agent can quickly generate load shedding commands according to the current state of the islanded microgrid, thus realizing efficient regulation of the system frequency, and this mode of offline training-online decision-making gives it a significant advantage in real-time computation. Furthermore, in contrast to strategy 3, strategy 1 proposes an improved DRL method, which introduces softmax into TD3, increases its replay buffer to three buffers, and classifies the stored experience samples. Through accurate value function estimation and learning of high-quality samples, it achieves precise fitting of model parameters, effectively improving the online inference speed of the model and reducing its online calculation time by 23.81% compared to strategy 3. Strategy 4 needs to sort the virtual combinations of the single-phase loads before determining the load shedding action, and then comprehensively evaluate the virtual three-phase load and other three-phase loads in various respects to determine the priority of the loads, and finally, use the agent to learn the optimal load shedding combination. This load shedding method for assessment and decision-making fails to make full use of the learning ability of the agent and has a longer response time in determining load shedding. The proposed strategy directly considers various load shedding-related factors, including the load frequency regulation effect, load importance, and three-phase unbalance degree, during the process of training the intelligent agent. Then, the trained intelligent agent is used to generate integrated load shedding decisions, thereby fully utilizing the learning ability of the intelligent agent while reducing the response time of load shedding decisions; this reduced its online computing time by 38.46% compared to strategy 4. In terms of frequency recovery time, the frequency recovery time of the system under the four strategies is 0.42 s, 0.58 s, 0.45 s, and 0.48 s, respectively. It can be seen that the system frequency under strategy 1 can recover to the normal range at the fastest speed, which is attributed to the fact that the TD3 after integrating the softmax and the DBR mechanism can make better load shedding decisions, and achieve the shortest online computation time based on further making high-quality decisions that are more conducive to the fast recovery of the system frequency, thus speeding up the frequency recovery speed. Based on achieving the shortest online computation time, TD3 can further formulate high-quality load shedding decisions that are more conducive to the rapid recovery of the system frequency, thus accelerating the frequency recovery

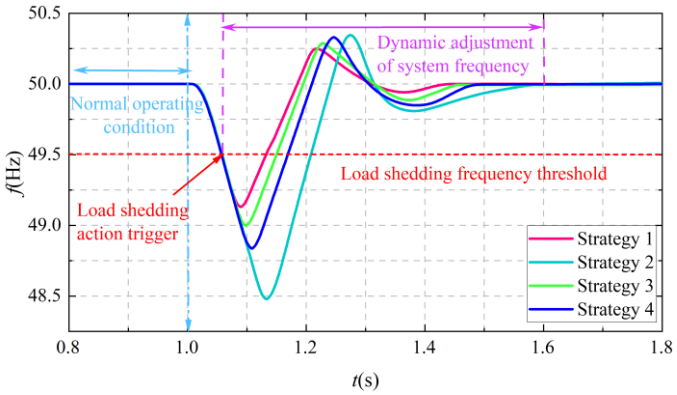

Fig. 9. System frequency recovery waveform under each strategy

Table VI
LOAD SHEDDING ACTION PERFORMANCE ANALYSIS

Index	Strategy 1	Strategy 2	Strategy 3	Strategy 4
t_{on}	0.032s	0.077s	0.042s	0.052s
t_{sum}	0.42s	0.58s	0.45s	0.48s
Δf	1.12Hz	1.87Hz	1.29Hz	1.49Hz

speed. Further analyzing the fluctuation of the system frequency during the recovery period, from Table VI, it can be seen that the amplitudes of the system frequency fluctuation under strategies 2, 3 and 4 during the recovery period are 1.87 Hz, 1.29 Hz and 1.49 Hz, respectively. In contrast, the frequency fluctuation range of the system under strategy 1 during the recovery period is 49.13 Hz–50.25 Hz, with a frequency fluctuation amplitude of only 1.12 Hz, which is 40.11%, 13.18%, and 24.83% lower than those of strategies 2, 3, and 4, respectively. This is mainly because in strategy 1, the load frequency regulation effect coefficient is considered in the integrated load shedding process, and a load with a small frequency regulation effect coefficient is preferentially removed, which effectively suppresses the decrease in system frequency and makes the system frequency recover to a normal state more stably.

The above results show that strategy 1 can realize a fast response when the system frequency falls to a threshold value, which meets the computational performance requirements for online real-time decision-making. At the same time, the load shedding strategy shows significant advantages in reducing both the amplitude of system frequency fluctuation and recovery time.

(4) Comparison of the Three-phase Unbalance During the Load Shedding Process

Considering that serious voltage unbalance will bring potential risks to the islanded microgrid system, the voltage unbalance degree of the islanded microgrid system is first analyzed. This section is also conducted under the fault scenario of BES3 exiting operation. The variation of voltage unbalance degree of islanded microgrid system in the process of underfrequency load shedding under various strategies is shown in Fig. 10. The maximum voltage unbalance of the islanded microgrid system before the load shedding operation is 1.1%. It can be seen from Fig. 10 that the voltage unbalance of the islanded microgrid system decreases after the load shedding actions under the four strategies are implemented. It can be seen that the system voltage unbalance degree in this fault scenario has been effectively controlled and

This article has been accepted for publication in a future issue of this journal, but has not been fully edited. Content may change prior to final publication.
Citation information: DOI: 10.1109/TSG.2025.3586757, IEEE Transactions on Smart Grid

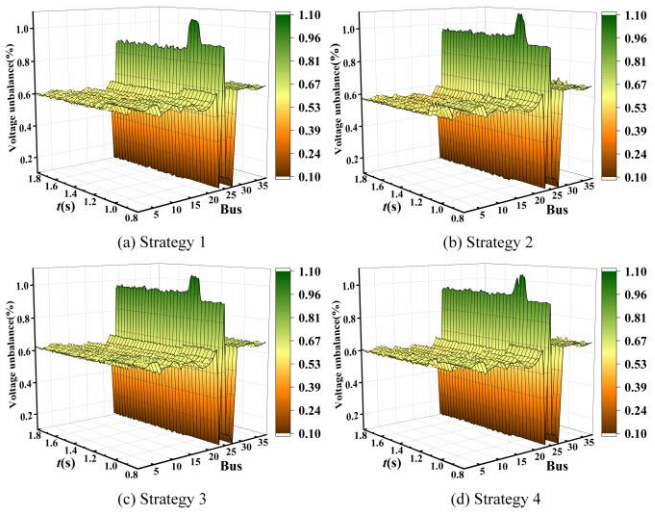

Fig. 10. Voltage unbalance variation of the islanded microgrid system under various strategies

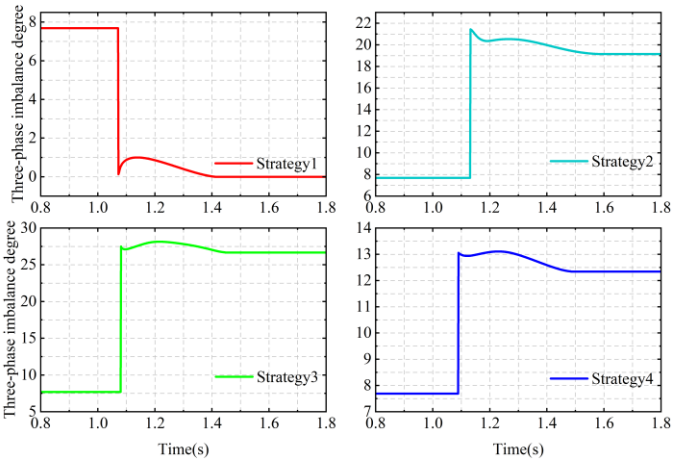

Fig. 11. Three-phase unbalance waveforms of the islanded microgrid system under various strategies

kept within the safe range of 3% [37], effectively avoiding the impact of serious voltage unbalance on the effectiveness of the case study.

To compare the three-phase power unbalance levels of islanded microgrids under different strategies, the three-phase unbalance degree of the system is calculated based on the three-phase power information. The waveform changes of the three-phase power unbalance in the islanded microgrid system during underfrequency load shedding actions under the various strategies are shown in Fig. 11.

According to Fig. 11, the three-phase unbalance degree of the islanded microgrid system before the load shedding operation is 7.69%. Because they do not consider the three-phase unbalance degree during the load shedding process, the three-phase unbalances of strategy 2 and strategy 3 after stable system operation was restored were 19.15% and 26.68%, respectively. Compared with that before the load shedding operation, the three-phase unbalance of the system increased by 11.46% and 18.99%, respectively, and exceeded the normal operation requirements of the system. ($Unbalance \leq 15\%$). Strategy 4 adopts a load combination approach to construct a single-phase load as a virtual three-phase load and then prioritizes cutting off the virtual three-phase loads with lower unbalances during the load shedding process to reduce the three-phase unbalance of the load shedding system. This load shedding method has an ideal effect in the scenario in which there is three-phase balance in the system before the fault occurs. However, when the system is initially in an unbalanced state, after cutting off a set of balanced virtual load combinations, strategy 4 increases the unbalance by 4.65%, reaching 12.34%. In contrast, the proposed strategy 1 reasonably distributes the load shedding each subphase by considering the three-phase unbalance of the load and corrects the three-phase unbalance of the system to 0, completely avoiding the impact of the three-phase unbalance on the system loss and load power quality.

In summary, compared with other strategies, the strategy proposed in this paper can minimize the load shedding cost on the premise that the voltage unbalance is lower than the safety threshold of 3%, and at the same time, the three-phase power unbalance of the system is corrected, and the system frequency is restored to the normal level faster and more stably, which verifies the superiority of the proposed strategy.

D. Robustness Analysis

From Section V-C, we conclude that the proposed integrated load shedding strategy has better load shedding performance than do the other comparative load shedding strategies. However, there will be state measurement noise in real power systems. To further verify the rationality and superiority of the proposed strategy, Gaussian white noise interference is added to the corresponding islanded microgrid environment state in each state detection step. The level of measured noise is described on the basis of the signal-to-noise ratio (SNR) in units of dB. Fig. 12 shows a comparison of the results of the proposed integrated load shedding strategy and the other strategies when BES3 exits due to faults under measurement noise levels of 5 dB, 10 dB, 15 dB, and 20 dB.

Fig. 12 shows that all the indicators of the four strategies are affected to some extent after noise is added. With increasing signal-to-noise ratio, the index performance of each strategy tends to improve. This is because the larger the signal-to-noise ratio is, the less noise is contained in the information; thus, the accuracy of each strategy in determining the state of the microgrid system is

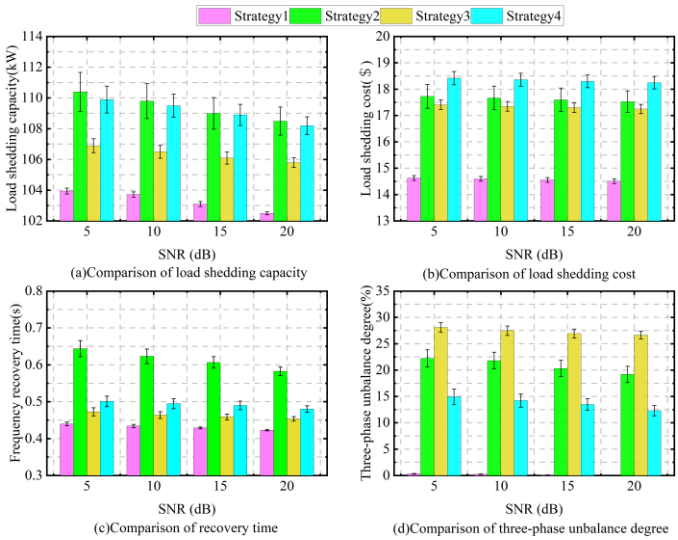

Fig. 12. Robustness comparison of strategies under noise

This article has been accepted for publication in a future issue of this journal, but has not been fully edited. Content may change prior to final publication.
Citation information: DOI: 10.1109/TSG.2025.3586757, IEEE Transactions on Smart Grid

less affected by noise, and the accuracy of underfrequency load shedding decisions is greater. The indexes of strategy 2 fluctuate the most under the influence of noise. In contrast, strategies 1, 3, and 4, as DRL-based load shedding strategies, choose the action that can obtain the maximum benefit each time, that is, the optimal load shedding strategy, and achieve better performance. Furthermore, compared with those of strategies 3 and 4, the differences in the load shedding, load shedding cost, recovery time and three-phase power unbalance degree of the proposed strategy 1 are 0.95 kW, \$0.12, 0.017 s, and 0.36%, respectively, in the 5 dB noise scenario and the 20 dB scenario. The differences from these four indicators for strategy 3 are 1.1 kW, \$0.16, 0.0192 s, and 1.46%, respectively. The differences from these four indicators for strategy 4 are 1.7 kW, \$0.17, 0.0204 s, and 2.61%, respectively. Although the load shedding indicators of the proposed strategy 1 are slightly increased under the influence of measurement noise, compared with those of strategies 3 and 4, they are still maintained at a lower level, and the fluctuations in the indicators are small. This shows that the proposed strategy 1 can better adapt to an uncertain environment and obtain more stable load shedding results.

The above test results indicate that compared with other strategies, the proposed integrated load shedding strategy can better cope with the measurement uncertainty of state variables such as the outputs of DG units in islanded microgrids, real-time powers of loads, real-time frequencies of microgrids, and frequency change rates. It can still obtain stable load shedding results under strong measurement noise interference. In the face of a changing islanded microgrid system environment, it has better robustness.

E. Generalization Performance Analysis

To further validate the generalization performance of the proposed strategy, a new fault scenario that is not involved in training is selected for testing. Assuming that DG6 and BES5 are simultaneously out of operation due to failure at 10:00, and the load level is 110% of the initial value. At this time, the withdrawal of DG and BES and the increase in load level will lead to a significant increase in the system power deficit, and the system frequency will face more serious disturbance. The maximum voltage unbalance and three-phase power unbalance of the islanded microgrid system before load shedding operation are 1.65% and 11.54%, respectively. In this scenario, the four strategies in Section V.C are still used for comparative analysis.

The composition of load shedding after the four load shedding strategies are implemented is shown in Fig. 13. The results show that strategy 1 has the smallest load shedding amount, only requiring the shedding of 205.6 kW of load. Compared with strategies 2, 3, and 4, the load shedding amount is reduced by 5.47%, 2.97%, and 4.46%, respectively. In this scenario, the four strategies all cut off part of level II important loads, but the proposed strategy 1 cut off the least level II important loads, thus ensuring the continuous power supply of high-priority loads to the maximum extent. In the selection of load shedding types, the load shedding objects of the four strategies all include industrial loads with high load demand at the current time, and the shedding amounts are 34.4kW, 40.3kW, 50.2kW and 52.5kW, respectively. Although the load shedding options of the four strategies will all have a certain impact on the user demand at this moment, the proposed strategy 1 minimizes the load shedding with high

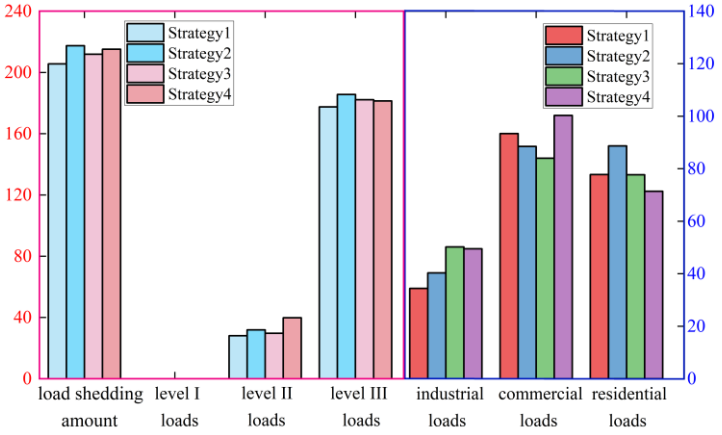

Fig. 13. Comparison of load shedding amount under different strategies

demand by considering multiclass factors including the load demand degree during the load shedding process and effectively alleviates the adverse impact on the user. It can be seen that strategy 1 performs better in ensuring the reliability of the power supply for important loads and high-demand loads.

The frequency recovery waveforms of the islanded microgrid system after load shedding under the four strategies are shown in Fig. 14. Due to the withdrawal of DG and BES and the increase of load level, the system frequency of the islanded microgrid fluctuates significantly. When the frequency drops to the threshold, the four strategies eliminate the system power shortage by formulating load shedding strategies in real-time, so that the system frequency returns to the normal range. The online calculation time, system frequency recovery time, and frequency fluctuation amplitude under each load shedding strategy are shown in Table VII. It can be intuitively observed that the proposed strategy 1 achieves the shortest online calculating time among all strategies, reducing it by 63.11%, 44.44%, and 51.09% compared to strategies 2, 3, and 4, respectively. This is because softmax and DBR mechanisms introduced in strategy 1 significantly improve the learning performance of the agent, and the trained model can realize more efficient forward reasoning by using DNN with more accurate parameter fitting in the online calculation stage, reducing redundant calculation and significantly improving the reasoning speed. At the same time, the integrated load shedding approach further reduces the transfer time between real-time load factor evaluation information and online decision-making, resulting in more efficient computing performance. In terms of frequency recovery time, strategy 1

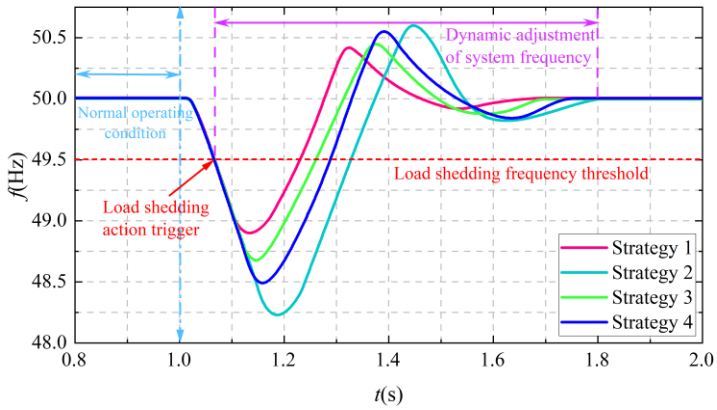

Fig. 14. System frequency recovery waveform under each strategy

This article has been accepted for publication in a future issue of this journal, but has not been fully edited. Content may change prior to final publication.
Citation information: DOI: 10.1109/TSG.2025.3586757, IEEE Transactions on Smart Grid

Table VII
LOAD SHEDDING ACTION PERFORMANCE ANALYSIS

Index	Strategy 1	Strategy 2	Strategy 3	Strategy 4
t_{on}	0.045s	0.122s	0.081s	0.092s
t_{sum}	0.64s	0.79s	0.68s	0.74s
Δf	1.51Hz	2.37Hz	1.77Hz	2.06Hz

Table VIII
LOAD REDUCTION CONTROL RESULTS

Index	Strategy 1	Strategy 2	Strategy 3	Strategy 4
g	\$225.78	\$296.8	\$235.57	\$346.2
VUF	1.43%	1.58%	1.49%	1.53%
Unbalance	9.78%	23.26%	28.49%	14.21%

based on DBR-SD3 has a higher quality of real-time load decision-making, and it can make the load shedding action that is most conducive to the stability of frequency recovery. It makes the frequency recovery time of the system under this strategy 0.64s, while the frequency recovery time of strategies 2, 3 and 4 are 0.79s, 0.68s, and 0.74s, respectively. Compared with the other three load shedding strategies, the frequency recovery time of proposed strategy 1 is reduced by 18.99%, 6.25%, and 13.51%, respectively, which indicates that strategy 1 is more conducive to the rapid recovery of system frequency. The frequency fluctuation amplitude of the islanded microgrid system under strategies 2, 3, and 4 are 2.37Hz, 1.77Hz, and 2.06Hz respectively. In contrast, strategy 1 retains more loads with a large frequency regulation effect coefficient in the process of the load removal and makes full use of the regulation effect of load itself in the process of frequency reduction. As a result, the amplitude of system frequency fluctuation of strategy 1 is 1.51Hz, which is 36.29%, 14.69%, and 26.7% lower than that of strategy 2, 3, and 4, respectively. The frequency fluctuation amplitude of the system is effectively suppressed. The above results show that strategy 1 can not only significantly reduce the amplitude of frequency fluctuation, but also accelerate the recovery of system frequency.

Under different load shedding strategies, the load shedding costs g, as well as the maximum voltage unbalance *VUF* and three-phase power unbalance *Unbalance* after the system stabilizes are shown in Table VIII. As can be seen from Table VIII, the four strategies can control the maximum voltage unbalance of the system within the safety threshold of 3%, avoiding the impact of voltage unbalance on the case study. In terms of load shedding costs, the load shedding costs of strategies 1, 2, 3, and 4 are \$225.78, \$296.8, \$235.57, and \$346.2 respectively. Strategy 1 considers both the importance level of the load and the demand for different types of loads during the load shedding process. It removes the load combination with the lowest cost coefficient, resulting in a reduction of load shedding costs by 23.93%, 4.16%, and 34.78% compared to strategies 2, 3, and 4, respectively. This minimizes the economic losses of load shedding. In terms of improving the three-phase power unbalance of the system, the three-phase power unbalance of the system after the implementation of strategies 2, 3, and 4 increased by 11.72%, 16.95%, and 2.67% respectively. Moreover, the load shedding actions under strategies 2 and 3 did not consider the power unbalance factor, which may affect the normal operation of the system after load removal. In contrast, strategy 1 corrects the power unbalance degree to 9.78%, which effectively reduces the influence of power unbalance on power quality.

According to the above test results, when facing untrained test scenarios, the agent can still make reasonable decisions and restore the system frequency to a stable state, which indicates that the model has a certain generalization ability. At the same time, the proposed strategy 1 is superior to strategies 2, 3, and 4 in reducing economic loss cost, inhibiting frequency fluctuation, shortening online calculation time and frequency recovery time, and improving three-phase power unbalance degree, showing better comprehensive load shedding effect. However, due to the difference between the training data distribution and the untrained fault scenario, the load shedding effect of strategy 1 in the untrained fault scenario has a certain degree of degradation. Compared with the training scenario in Section V.C, the online calculation time, system frequency recovery time, and fluctuation amplitude of the proposed strategy 1 increased by 40.63%, 52.38%, and 34.82%, respectively. The above results show that the model has some shortcomings in adaptability when dealing with unfamiliar fault environments, and the decision-making

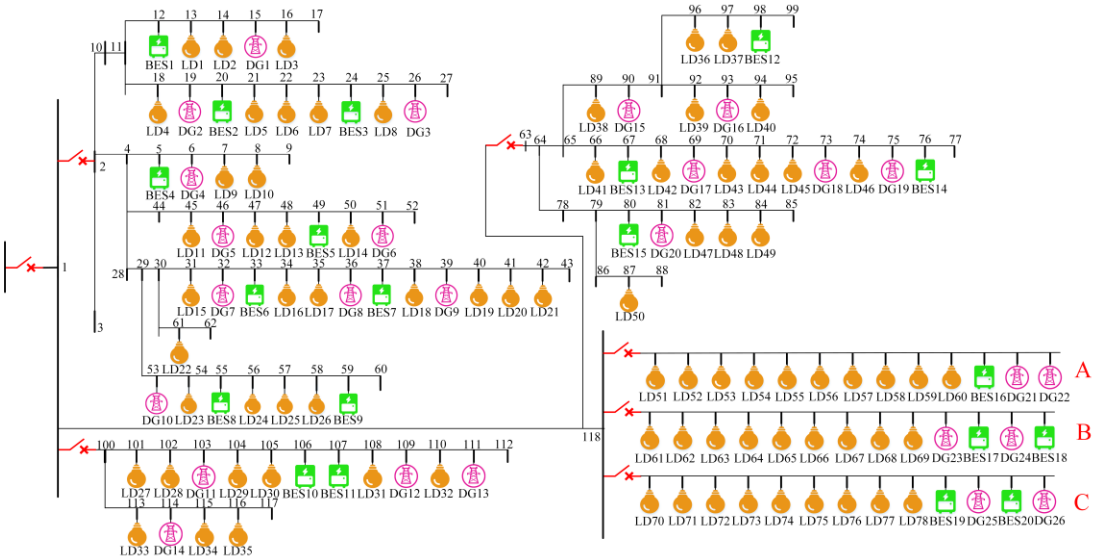

Fig. 15. Improved IEEE 118-bus island microgrid system model

This article has been accepted for publication in a future issue of this journal, but has not been fully edited. Content may change prior to final publication.
Citation information: DOI: 10.1109/TSG.2025.3586757, IEEE Transactions on Smart Grid

ability of agents under unknown conditions needs to be further improved.

F. Superiority Analysis of Load Shedding Strategies in IEEE 118-bus System

To further analyze the load shedding performance of the proposed strategy in larger-scale systems, an islanded microgrid model based on the improved IEEE 118-bus system is established in MATLAB/Simulink, as shown in Fig. 15. The model consists of 26 DGs, 20 BES, and 78 loads. BES1-BES20 operates in grid-forming mode, while DG1-DG26 operates in grid-following mode. Among them, LD1-LD50 are three-phase loads, and LD51-LD78 are single-phase loads. The DG and BES output information are shown in TABLE IX, and the load grades and load types are shown in TABLE X. The load demand degrees at different times remain consistent with the data in Fig. 6.

Assuming DG9 exits operation due to a fault at 20:00, with a load level of 105%. The maximum voltage unbalance and three-phase power unbalance of the islanded microgrid system before load shedding operation are 1.98% and 12.18%, respectively. In this scenario, the four load shedding strategies from Section V.C are used for comparative analysis.

Table IX
DG AND ENERGY STORAGE CONFIGURATION INFORMATION

Name	Access Location	Output (kW)	Name	Access Location	Output (kW)
DG1	Bus 15	7	DG24	Bus 118-B	11.5
DG2	Bus 19	3	DG25	Bus 118-C	23
DG3	Bus 26	3	DG26	Bus 118-C	14
DG4	Bus 6	5	BES1	Bus 12	5
DG5	Bus 46	5	BES2	Bus 20	4
DG6	Bus 51	21	BES3	Bus 24	3
DG7	Bus 32	8.3	BES4	Bus 5	3
DG8	Bus 36	7	BES5	Bus 49	3
DG9	Bus 39	35	BES6	Bus 33	4
DG10	Bus 53	12	BES7	Bus 37	10
DG11	Bus 103	26.5	BES8	Bus 55	20
DG12	Bus 109	13	BES9	Bus 59	3
DG13	Bus 111	11.5	BES10	Bus 106	3
DG14	Bus 114	12	BES11	Bus 107	10
DG15	Bus 90	14	BES12	Bus 98	3
DG16	Bus 93	12.5	BES13	Bus 67	3
DG17	Bus 69	30	BES14	Bus 76	4
DG18	Bus 73	14	BES15	Bus 80	20
DG19	Bus 75	13.5	BES16	Bus 118-A	5
DG20	Bus 81	15	BES17	Bus 118-B	5
DG21	Bus 118-A	13.5	BES18	Bus 118-B	8
DG22	Bus 118-A	20.5	BES19	Bus 118-C	5
DG23	Bus 118-B	12	BES20	Bus 118-C	8

Table X
LOAD DATA INFORMATION

Load	Priority	P^L (kW)	h(\$/kWh)	$P^{cut,\max}$ (kW)	Load type
LD1	II	5.5	1.21	2.5	commercial
LD2	I	3	2.46	1.2	industrial
LD3	III	5.5	0.56	2.1	residential
LD4	I	4.8	3.01	1.5	commercial
LD5	II	4.1	2.27	2.1	industrial
LD6	II	17.5	1.94	11.7	residential
LD7	II	5.6	2.31	2.8	commercial
LD8	III	2.2	0.98	1.3	residential
LD9	III	3.1	1.84	1.7	industrial
LD10	I	6.6	2.25	2.2	commercial
LD11	III	7.1	1.05	4.3	industrial
LD12	II	4.5	2.16	2.5	residential
LD13	I	5.3	2.71	2.1	industrial
LD14	III	2.9	1.69	1.4	commercial
LD15	III	3.6	1.26	2.2	residential
LD16	II	4.2	2.72	2.1	industrial
LD17	III	7.8	0.97	4.2	industrial
LD18	I	5.2	2.75	2.2	residential
LD19	III	8.7	1.03	2.1	commercial
LD20	II	8.9	2.41	7.5	commercial
LD21	III	4.8	1.42	3.2	residential
LD22	II	8.6	1.51	5.1	commercial
LD23	I	6.3	2.63	2.8	commercial
LD24	III	5.7	0.99	3.2	industrial
LD25	III	5.5	1.2	2.5	commercial
LD26	II	3.3	1.62	1.7	residential
LD27	I	5.8	3.04	2.4	industrial
LD28	II	3.9	2.54	2.1	commercial
LD29	III	3.8	1.24	2.5	industrial
LD30	II	7.6	0.79	3.3	residential
LD31	III	4.9	1.21	2.8	industrial
LD32	II	4.5	1.36	2.1	commercial
LD33	I	5.3	2.77	2.2	residential
LD34	III	8.6	0.81	5.6	commercial
LD35	III	15.8	0.37	10.5	residential
LD36	II	4.9	1.41	3.1	commercial
LD37	II	3.4	1.96	2.4	industrial
LD38	III	7.8	0.56	5.8	commercial
LD39	I	7.2	2.81	3.3	industrial
LD40	I	6.3	3.07	3.1	commercial
LD41	III	5.9	1.24	3.2	residential
LD42	II	7.2	1.58	4.6	commercial
LD43	III	9.1	0.64	7.2	industrial
LD44	III	8.6	0.71	6.6	commercial
LD45	III	5.4	1.06	4.1	residential
LD46	II	5.5	1.55	3.5	industrial
LD47	I	9.8	2.76	4.5	commercial
LD48	III	8.3	0.87	6.8	industrial
LD49	II	7.8	1.34	4.2	commercial
LD50	II	7.9	1.22	4.0	residential
LD51	II	9.3	1.41	7.6	commercial
LD52	III	5.3	0.86	3.9	commercial
LD53	III	4.8	0.71	3.1	industrial
LD54	I	9.6	2.58	8.5	residential
LD55	III	5.3	0.96	4.7	industrial
LD56	II	3.6	1.54	2.2	commercial
LD57	III	1.1	1.02	0.5	industrial
LD58	I	2.1	2.63	1.1	residential
LD59	III	7.9	0.91	6.1	industrial
LD60	II	6.1	1.32	5.1	industrial
LD61	III	8.3	0.97	6.9	commercial
LD62	III	4.7	1.15	3.3	industrial
LD63	II	8.2	1.39	6.6	residential
LD64	I	5	2.11	3.9	industrial
LD65	III	6.8	1.01	5.2	commercial
LD66	III	3.6	0.79	2.4	residential
LD67	II	8.5	1.36	6.2	commercial
LD68	III	2.8	0.85	1.6	residential
LD69	I	2.2	1.96	1.6	commercial
LD70	II	6.7	1.52	5.4	commercial
LD71	III	5.5	0.67	3.2	industrial
LD72	II	6.8	1.44	5.5	commercial
LD73	II	8.9	1.49	7.7	residential
LD74	I	7.1	2.59	5.6	commercial
LD75	III	4.5	0.99	2.9	commercial
LD76	I	6.3	1.32	4.9	industrial
LD77	II	7.9	1.46	6.1	commercial
LD78	III	5.5	0.82	3.9	industrial

The composition of load shedding after the four load shedding strategies are implemented is shown in Fig. 16. Strategy 1 achieved the minimal load shedding amount and the lowest shedding amount of level II loads, indicating its ability to maximize power supply reliability for critical loads while minimizing overall load shedding amount. Further analysis of the removal of various types of loads shows that strategies 2, 3, and 4 remove residential loads with high demand degree, accounting for 22.67%, 21.4%, and 23.34% of the load shedding amount,

This article has been accepted for publication in a future issue of this journal, but has not been fully edited. Content may change prior to final publication.
Citation information: DOI: 10.1109/TSG.2025.3586757, IEEE Transactions on Smart Grid

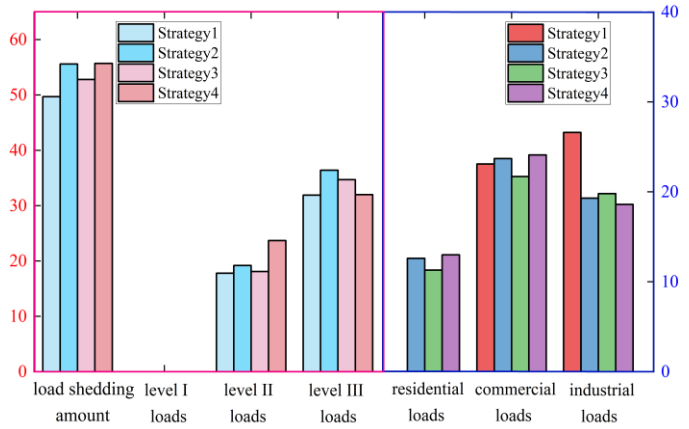

Fig. 16 Comparison of load shedding amount under different strategies

respectively.

In contrast, strategy 1 takes into account the differences in demand among users for different types of loads, and prioritizes the reduction of load on commercial and industrial loads with lower demand at the current time, effectively avoiding the cutting off of high-demand residential loads and minimizing the negative impact of load shedding on the user level. These results demonstrate that strategy 1 significantly enhances the continuous power supply capability for critical and high-demand loads in large-scale islanded microgrids. The above results indicate that compared to the other three strategies, strategy 1 can still effectively improve the sustained power supply capacity of important loads and high demand loads in the face of larger islanded microgrid system failure scenarios, further verifying the superiority of the proposed strategy 1.

The fault occurrence time is set to t=1 s in the modified IEEE 118-bus model. The frequency recovery waveforms of the islanded microgrid system after load shedding under the four strategies are shown in Fig. 17. The online calculation time t_{on}, system frequency recovery time t_{sum}, and frequency fluctuation amplitude Δf under each load shedding strategy are shown in Table XI.

As shown in Fig. 17, after DG9 exits operation due to a fault, the system experiences a frequency drop caused by a power deficit. All four strategies respond in real time and generate load shedding schemes online. In terms of online calculation time, the calculation times for the four strategies are 0.092s, 0.168s, 0.102s, and 0.118s, respectively. The load shedding method based on MPC in strategy 2 is more complex and computationally intensive when dealing with large-scale bus systems due to the need to optimize more decision variables, resulting in the longest solution time and certain limitations in real-time performance. However, strategies 1, 2, and 3 based on DRL can achieve less online calculation time through trained agent models. Furthermore, the softmax and DBR mechanisms introduced in strategy 1 can enhance the learning efficiency of the agent, while the integrated load shedding method avoids the delayed response caused by online evaluation. This reduces the real-time calculation time of strategy 1 by 9.8% and 22.03% respectively compared to strategy 3 and strategy 4, effectively shortening the speed of model output for online decision-making. In terms of frequency recovery time, the frequency recovery time of the four strategies is 0.78s, 0.96s, 0.85s, and 0.89s, respectively. It can be seen that compared with the other three strategies, the frequency recovery time of strategy 1 is reduced by 18.78%, 8.24%, and 12.36%, respectively. This indicates that the load shedding action taken by strategy 1 is superior to the other three strategies and more conducive to the rapid recovery of system frequency. When executing the load shedding action, strategy 1 prioritizes cutting off loads with small frequency regulation effect coefficients, maximizing the utilization of the load's regulation effect, resulting in a frequency fluctuation of 1.74Hz in the system. The frequency fluctuations in strategies 2, 3, and 4 are 2.55Hz, 1.91Hz, and 2.2Hz, respectively. Compared to strategies 2, 3, and 4, strategy 1 can reduce the amplitude of frequency fluctuations by 31.76%, 8.9%, and 20.91%, respectively, effectively reducing fluctuations during frequency recovery. The above analysis results indicate that strategy 1 can better meet the requirements of online real-time calculating performance, while effectively reducing the frequency fluctuation amplitude and frequency recovery time of islanded microgrids.

Under different load shedding strategies, the load shedding costs g, as well as the maximum voltage unbalance VUF and three-phase power unbalance $Unbalance$ after the system stabilizes are shown in Table XII. It can be seen from Table XII that after the implementation of the four load shedding strategies, the maximum voltage unbalance of the system is maintained within the safe range of 3%. In terms of load shedding costs, strategy 1 has a load shedding cost of $199.26, which is the lowest among the four strategies, reducing 16.45%, 10.51%, and 28.04% compared to strategies 2, 3, and 4, respectively. Regarding three-phase power unbalance improvement, strategies 2 and 3 do not consider power unbalance impacts during decision-making, leading to increases of 14.58% and 19.24% compared to pre-shedding levels. In contrast, strategies 1 and 4 consider the

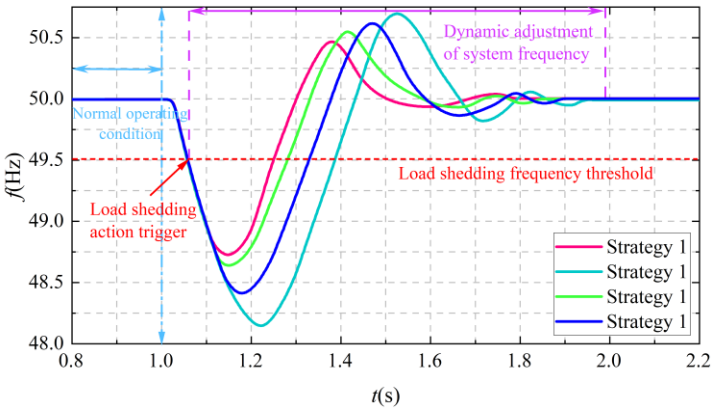

Fig. 17. System frequency recovery waveform under each strategy

Table XI
LOAD SHEDDING ACTION PERFORMANCE ANALYSIS

Index	Strategy 1	Strategy 2	Strategy 3	Strategy 4
t_{on}	0.092s	0.168s	0.102s	0.118s
t_{sum}	0.78s	0.96s	0.85s	0.89s
Δf	1.74Hz	2.55Hz	1.91Hz	2.2Hz

Table XII
LOAD REDUCTION CONTROL RESULTS

Index	Strategy 1	Strategy 2	Strategy 3	Strategy 4
g	$199.26	$238.50	$222.65	$276.9
VUF	1.62%	1.83%	1.71%	1.78%
$Unbalance$	6.39%	26.76%	31.42%	13.54%

power unbalance factor in the decision-making of load shedding and control the unbalance degree within the normal range. Furthermore, strategy 1 allocates the load shedding amount on each single phase reasonably through an integrated load shedding mode under the initial unbalance of the system, thereby reducing the power unbalance of the system to 6.39%, achieving the minimization of power unbalance under the four strategies. From the above analysis, it can be seen that strategy 1 can minimize the economic losses caused by load shedding while ensuring that voltage unbalance is within a safe range, and control power unbalance at the lowest level.

From the above analysis, it can be seen that the proposed strategy 1 can effectively solve the frequency recovery problem in larger islanded microgrid systems. Meanwhile, compared to the other three strategies, the proposed strategy 1 can minimize the cost of load shedding, while demonstrating significant advantages in reducing frequency fluctuations, shortening frequency recovery time, and improving three-phase power unbalance. This further validates the superiority of the proposed strategy.

VI. CONCLUSION

Considering the frequency drop caused by unexpected faults during the operation of islanded microgrids, this paper presents an integrated underfrequency load shedding strategy for islanded microgrids by integrating multiclass load-related factors on the basis of the DRL framework. The strategy first combines load assessment and load shedding to construct an integrated underfrequency load shedding strategy integrating multiclass load correlation factors. Then, the integrated load shedding model is described as an MDP with the goal of minimizing the load shedding response time, load shedding cost, and three-phase system power unbalance, and a DBR-SD3 method based on a continuous action space is proposed to determine the optimal load shedding strategy for this objective. By integrating the softmax function and dual-buffer replay mechanism into TD3, this method greatly improves the ability of the agent to learn the optimal load shedding strategy in the complex microgrid operating environment. Finally, simulation and comparison tests are carried out on the improved IEEE 37-bus and IEEE 118-bus islanded microgrid system. The results show that the proposed strategy can prevent a rapid drop in the system frequency through the integrated load shedding decision and can achieve a low load shedding cost to ensure the reliability of the power supplies of important loads while correcting the three-phase power unbalance in system operation. In addition, this strategy has greater robustness and adaptability in a complex microgrid system environment.

REFERENCES

[1] C. Wang *et al*., "Strategy for optimizing the bidirectional time-of-use electricity price in multi-microgrids coupled with multilevel games," *Energy*, vol. 323, no. 135731, May. 2025.

[2] Z. Zhao, J. Xu, Y. Lei, C. Liu, X. Shi and L. Lai, "Robust dynamic dispatch strategy for multi-uncertainties integrated energy microgrids based on enhanced hierarchical model predictive control," *Appl. Energy*, vol. 381, no. 125141, Mar. 2025.

[3] Y. Zeng, Q. Yang, Y. Lin, Y. Chen, X. Chen and J. Wen, "Fractional-Order Virtual Inertia Control and Parameter Tuning for Energy-Storage System in Low-Inertia Power Grid," *Protection and Control of Modern Power Systems*, vol. 9, no. 5, pp. 70-83, Sept. 2024.

[4] S. Zhao *et al*., "Unreliability Tracing of Power Systems for Identifying the Most Critical Risk Factors Considering Mixed Uncertainties in Wind Power Output," *Protection and Control of Modern Power Systems*, vol. 9, no. 5, pp. 96-111, Sept. 2024.

[5] Y. Liu, Z. Li and J. Zhao, "Safety-Constrained Stagewise Optimization of Droop Control Parameters for Isolated Microgrids," *IEEE Trans. Smart Grid*, vol. 15, no. 1, pp. 77-88, Jan. 2024.

[6] L. He, Z. Tan, Y. Li, Y. Cao and C. Chen, "A Coordinated Consensus Control Strategy for Distributed Battery Energy Storages Considering Different Frequency Control Demands," *IEEE Trans. Sustainable Energy*, vol. 15, no. 1, pp. 304-315, Jan. 2024.

[7] S. M. Rostami and M. Hamzeh, "An Adaptive Multi-Functional Control Strategy for Power Management and Voltage-Frequency Regulation of PV, BESS, and Hybrid Units in a Microgrid," *IEEE Trans. Smart Grid*, vol. 15, no. 4, pp. 3446-3458, Jul. 2024.

[8] C. Wang *et al*., "A two-stage underfrequency load shedding strategy for microgrid groups considering risk avoidance," *Appl. Energy*, vol. 367, no. 123343, Aug. 2024.

[9] F. Huang *et al*., "Integrated emergency control strategy for single/three-phase hybrid microgrid group coupling load correlation factors and under-frequency load shedding," *Electr. Power Syst. Res.*, vol. 242, no. 111481, May. 2025.

[10] T. Amraee, A.M. Ranjbar, and R. Feuillet, "Adaptive under-voltage load shedding scheme using model predictive control," *Electr. Power Syst. Res.*, vol. 81, no. 7, pp. 1507-1513, Jul. 2011.

[11] J. Tang, J. Liu, F. Ponci and A. Monti, "Adaptive load shedding based on combined frequency and voltage stability assessment using synchrophasor measurements," *IEEE Trans. Power Syst.*, vol. 28, no. 2, pp. 2035-2047, May 2013.

[12] D. G. Mohammad and A. Turaj, "Dynamic multi-stage under frequency load shedding considering uncertainty of generation loss," *IET Gener. Transm. Distrib.*, vol. 11, no. 13, pp. 3202-3209, Sept. 2017.

[13] C. Wang *et al*., "Multiagent deep reinforcement learning-based cooperative optimal operation with strong scalability for residential microgrid clusters," *Energy*, vol. 314, no. 134165, Jan. 2025.

[14] W. Zhao, T. Zeng, Z. Liu, L. Xie, L. Xi and H. Ma, "Automatic Generation Control in a Distributed Power Grid Based on Multi-Step Reinforcement Learning," *Protection and Control of Modern Power Systems*, vol. 9, no. 4, pp. 39-50, Jul. 2024.

[15] A. K. Singh and M. Fozdar, "Event-driven frequency and voltage stability predictive assessment and unified load shedding," *IET Gener., Transmiss. Distrib*., vol. 13, no. 19, pp. 4410–4420, 2019.

[16] Y. Dai, Y. Xu, Z. Dong, K. Wong and L. Zhuang, "Real-time prediction of event-driven load shedding for frequency stability enhancement of power systems," *IET Gener., Transmiss. Distrib.*, vol. 6, no. 9, pp. 914–921, 2012.

[17] C. Li et al., "Continuous under-frequency load shedding scheme for power system adaptive frequency control," *IEEE Trans. Power Syst.*, vol. 35, no. 2, pp. 950–961, Mar. 2020.

[18] C. Wang, S. Mei, Q. Dong, R. Chen and B. Zhu, "Coordinated load shedding control scheme for recovering frequency in islanded microgrids," *IEEE Access*, vol. 8, pp. 215388-215398, 2020.

[19] Q. Huang, R. Huang, W. Hao, J. Tan, R. Fan and Z. Huang. "Adaptive power system emergency control using deep reinforcement learning," *IEEE Trans. Smart Grid*, vol. 11, no. 2, pp. 1171-1182, Mar. 2020.

[20] C. Chen, M. Cui, F. Li, S. Yin and X. Wang, "Model-Free Emergency Frequency Control Based on Reinforcement Learning," *IEEE Trans. Ind. Inf.*, vol. 17, no. 4, pp. 2336-2346, Apr. 2021.

[21] P. Chen and D. Han, "Reward adaptive wind power tracking control based on deep deterministic policy gradient," *Appl. Energy*, vol. 348, no. 121519, Oct. 2023.

[22] J. Li and Y. Cheng, "Deep Meta-Reinforcement Learning-Based Data-Driven Active Fault Tolerance Load Frequency Control for Islanded Microgrids Considering Internet of Things," *IEEE Internet Things. J*, vol. 11, no. 6, pp. 10295-10303, Mar. 2024.

[23] R. Wang, S. Bu and C. Y. Chung, "Real-Time Joint Regulations of Frequency and Voltage for TSO-DSO Coordination: A Deep Reinforcement Learning-Based Approach," *IEEE Trans. Smart Grid*, vol. 15, no. 2, pp. 2294-2308, Mar. 2024.

[24] B. Fan, X. Liu, G. Xiao, X. Yang, B. Chen and P. Wang, "Enhancing Adaptability of Restoration Strategy for Distribution Network: A Meta-Based Graph Reinforcement Learning Approach," *IEEE Internet Things. J*, vol. 11, no. 14, pp. 25440-25453, Jul. 2024

[25] C. Wang, X. Li, T. Tian, Z. Xu and R. Chen, "Coordinated control of passive transition from grid-connected to islanded operation for three/single-phase hybrid multimicrogrids considering speed and smoothness," *IEEE Trans. Ind. Electr.*, vol. 67, no. 3, pp. 1921-1931, Mar. 2020.

[26] C. Wang, S. Chu, H. Yu, Y. Ying and R. Chen, "Control strategy of unintentional islanding transition with high adaptability for three/single-phase hybrid multimicrogrids," *Int. J. Electr. Power Energy Syst.*, vol. 136, no. 107724, Mar. 2022.
[27] C. Wang *et al*., "Underfrequency Load Shedding Scheme for Islanded Microgrids Considering Objective and Subjective Weight of Loads," *IEEE Trans. Smart Grid*, vol. 14, no. 2, pp. 899-913, Mar. 2023.
[28] A. Bokhari *et al*., "Experimental determination of the ZIP coefficients for modern residential, commercial, and industrial loads," *IEEE Trans. Power Deli.*, vol. 29, no. 3, pp. 1372-1381, Jun. 2014.
[29] L. Yang, X Cui, Y Qin, "Emergency power supply scheme and fault repair strategy for distribution networks considering electric -traffic synergy," *Sustain. Energy Grids Netw.*, vol. 40, no. 101575, Dec. 2024.
[30] C. Wang, S. Mei, H. Yu, S. Cheng, L. Du and P. Yang, "Unintentional Islanding Transition Control Strategy for Three-/Single-Phase Multimicrogrids Based on Artificial Emotional Reinforcement Learning," *IEEE Syst. J*, vol. 15, no. 4, pp. 5464-5475, Dec. 2021.
[31] Z. Xu, P. Yang, Y. Zhang, S. Song and Z, Zhao, "Day-Ahead Economic Optimized Dispatch of Single and Three Phase Hybrid Multi-Microgrid Considering Unbalance Constraint," *Power System Technology*, vol. 41, no. 1, pp. 40-47, Jan. 2017.
[32] C. Jiang, L. Zheng, C. Liu, F. Chen and Z. Shao, "MADDPG-Based Active Distribution Network Dynamic Reconfiguration with Renewable Energy," *Protection and Control of Modern Power Systems*, vol. 9, no. 6, pp. 143-155, Nov, 2024.
[33] C. Wang *et al*., "Prioritized sum-tree experience replay TD3 DRL-based online energy management of a residential microgrid," *Appl. Energy*, vol. 368, no. 123471, Aug. 2024.
[34] H. Wang, Z. Chen, H. Zhao and Y. Yue, "Reconstruction strategies for fault recovery of active distribution network with distributed generation uncertainties," *Power System Technology*, vol. 46, no. 11, pp. 4356-4364, Nov. 2022.
[35] C. Wang, Q. Dong, S. Mei, X. Li, S. Kang and H. Wang, "Seamless transition control strategy for three/single-phase multimicrogrids during unintentional islanding scenarios," *Int. J. Electr. Power Energy Syst.*, vol. 133, no. 107257, Dec. 2021.
[36] S. Mohammad, S. Kalajahi, H. Seyedi and K. Zare, "Under-frequency load shedding in isolated multi-microgrids," *Sustain Energy Grids*, vol. 27, no. 100494, Sep. 2021.
[37] Q. Xiao *et al*., "Assessment of Transmission-level Fault Impacts on 3-phase and 1-phase Distribution IBR Operation," *2024 IEEE Power & Energy Society General Meeting (PESGM)*, Seattle, WA, USA, pp. 1-5, 2024.

Can Wang (Member, IEEE) was born in Hubei, China. He received the Ph.D. degree in electrical engineering from the South China University of Technology, Guangzhou, China, in 2017.He is currently an Associate Professor of Electrical Engineering with the College of Electrical Engineering and New Energy, China Three Gorges University, Yichang, China. His current research interests include distributed generation, microgrid operation and control, integrated energy system, and smart grids. He serves as the Co-Chair of the Special Session on "Power Systems With Penetration of RE and EV" in IEEE IGBSG 2019. He is also a member of the Youth Editorial Committee of Electric Power, Electric Power Construction, Journal of Electric Power Science and Technology, and Protection and Control of Modern Power Systems.

He is an Active Reviewer of IEEE Transactions on Smart Grid, IEEE Transactions on Sustainable Energy, IEEE Transactions on Industrial Electronics, IEEE Transactions on Industrial Informatics, Applied Energy, Energy, Energies, and IEEE Access.

Bentao Cheng was born in Hubei, China. He is currently working toward the M.S. degree in electrical engineering with China Three Gorges University, Yichang, China. His research interests include distributed generation and microgrid operation and control.

Xuhui He was born in Hubei, China. He received his M.S. degree in electrical engineering with China Three Gorges University, Yichang, China. His research interests include distributed generation and operation optimization of smart grid.

Lei Xi (Member, IEEE) received the M.S. degree in control theory and control engineering from the Harbin University of Science and Technology, Harbin, China, in 2009, and the Ph.D. degree in electrical engineering from the South China University of Technology, Guangzhou, China, in 2016. He is currently a Full Professor with the College of Electrical Engineering and New Energy, China Three Gorges University, Yichang, China. His research interests include the load frequency control, artificial intelligence techniques, automatic generation control and network attack and defense.

Nan Yang (Senior Member, IEEE) received the B.S. degree in electrical engineering from Taiyuan University of Technology, Taiyuan, China, in 2009, and the Ph.D. degree in electrical engineering from Wuhan University, Wuhan, China, in 2014. He is currently an Associate Professor with the College of Electrical Engineering and New Energy, China Three Gorges University, Yichang, China. His major research interests include power dispatching automation of new energy sources, artificial intelligence, planning and operation of power systems, operation and control of microgrid, and active distribution networks.

Zhouli Zhao (Member, IEEE)) received the Ph.D. degree in electrical engineering from the South China University of Technology, Guangzhou, China, in 2017. From 2014 to 2015, he was a Joint Ph.D. Student and Sponsored Researcher with the Control and Power Research Group, Department of Electrical and Electronic Engineering, Imperial College London, London, U.K. From 2017 to 2018, he was a Research Associate with the Smart Grid Research Laboratory, Electric Power Research Institute, China Southern Power Grid, Guangzhou, China. He is currently an Associate Professor with the School of Automation, Guangdong University of Technology, Guangzhou, China. His research interests include microgrid control and energy management, renewable power generation control, and smart grids.

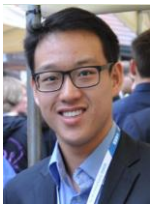

Chun Sing Lai (Senior Member, IEEE) received the B.Eng. (First Class Hons.) in electrical and electronic engineering from Brunel University London, London, U.K., in 2013, and the D.Phil. degree in engineering science from the University of Oxford, Oxford, U.K., in 2019. He is with the Department of Electronic and Electrical Engineering, Brunel University London and also with the Department of Electrical Engineering, School of Automation, Guangdong University of Technology. His major research interests include power dispatching automation of new energy sources, power system optimization, energy system modeling, operation and control of microgrid, and active distribution networks.

Loi Lei Lai (Life Member, IEEE) received the B.Sc. (First Class Hons.), Ph.D., and D.Sc. degrees in electrical and electronic engineering from the University of Aston, Birmingham, U.K., and City, University of London, London, U.K., in 1980, 1984, and 2005, respectively. Professor Lai is currently a University Distinguished Professor with the Guangdong University of Technology, Guangzhou, China. He was a Pao Yue Kong Chair Professor with Zhejiang University, Hangzhou, China, and the Professor and Chair of Electrical Engineering with City, University of London. His major research interests include power system under high penetration of renewables, smart energy network, operation and control of microgrid, and active distribution networks.